On the problem of Variational Assimilation of Precipitation Data Using Moist-Convective Parameterization Schemes

Luc Fillion
Atmospheric Environment Service, Dorval, Québec, Canada

Ronald Errico
National Center for Atmospheric Research, Boulder, Colorado, USA

Summary: Some basic aspects related to the problem of incorporating moist-convective processes in a variational data assimilation framework are considered. The methodology is based on inverse problem theory and is formulated in its simplest context where the adjustment of temperature and humidity fields take place in the vertical only. In contrast to previous studies on the subject, the impact of error statistics from prior and data sources of information is clarified. The accuracy of linearization of convection operators and the resulting impact in a minimization procedure are examined. Versions of two schemes are examined: the Kuo-Anthes scheme and the Relaxed Arakawa-Schubert scheme (RAS).

1. Introduction

The current status at most operational Numerical Weather Prediction (NWP) centers is that the humidity field is still univariately analysed without coupling (at the analysis time) with dynamical and physical processes. This situation is expected to change significantly in the near future however. Following the success of introduction of *dynamical* processes within newly developed variational analysis schemes, and the now growing interest in treating physical processes, it is justified at this time to clarify the role of moist-convective parameterization schemes in a variational data assimilation framework. The most ambitious plan is to consider the problem within a four-dimensional variational data assimilation procedure (4D-Var) directly. This represents however a

significant step ahead that has been explored during the last years (e.g. Zou et al. 1993; Zupanski and Mesinger 1995; Tsuyuki 1996a,b).

There is still much to be understood before reliable introduction of moist-convection into variational analysis schemes can be done. Properly treating discontinuities form an essential part of the problem (e.g.Vukicevic and Errico 1993; Zupanski, D. 1993; Xu 1996a,b). The non-linear behavior of these processes is also an important aspect that needs further examination. The present study rather concentrates on the nature of the adjustment on temperature and specific-humidity fields resulting from a one-dimensional variational assimilation (1D-Var) of precipitation-rate data, where moist-convection is the dominant process. The specific objectives of our study are to examine the following points:

(1) Columnwise sensitivity and non-linearity of moist-convective parameterization schemes

(2) Details about the nature of adjustments of background profiles

(3) Behavior of the minimization in the vicinity of saturated states

(4) Variability of points (2) and (3) in terms of different parameterization schemes. For instance, how does the vertical structure of analysis increments on temperature vary in terms of the moist-convective scheme used. This has implications for the resulting dynamical balance.

(5) Impact of background-error statistics. Implications for dynamical balance.

Section 2 introduces the analysis problem. In Section 3 we describe the essentials of the Kuo-Anthes and Relaxed Arakawa-Schubert (RAS) convective parameterization schemes used in this study. Section 4 gives the details of the numerical implementation of the 1D-Var problem together with the set of statistics and background fields used. The ensemble of results clarifying points (1) - (5) above are given in Section 5.

2. The 1D-Var problem

Consider the following variational problem

$$\min \quad J(\mathbf{x}) = \frac{1}{2}[\mathbf{x} - \mathbf{x}^b]^T \mathbf{B}^{-1}[\mathbf{x} - \mathbf{x}^b] + \frac{1}{2}[H(\mathbf{x}) - \mathrm{y}^o]^T \mathrm{R}^{-1}[H(\mathbf{x}) - \mathrm{y}^o] \qquad (1)$$

where

$\mathbf{x} = (\mathbf{T}, \mathbf{q})^{\mathrm{T}}$: State-vector of dimension $\mathrm{N} = 2\mathrm{N_k}$, where $\mathrm{N_k}$ is the number of vertical levels and **T**, **q** are vectors of vertical profiles of temperature and specific humidity at a given geographical point.

$\mathbf{x}^b$: Background state-vector at the observation location

y^{o} : Instantaneous precipitation-rate data where moist-convection is assumed to occur and deduced from SSMI or Radar instruments for instance.

B : A-priori (background) error covariance matrix.

R : Observational error variance.

H : Non-linear observation operator.

The first and second right-hand-side terms of (1) will be referred to as the "background term" $\mathrm{J_b}$, and the "observational term" $\mathrm{J_o}$ respectively. Given a state-vector **x,** we assume that the precipitation is of convective nature and we disregard large-scale precipitation processes. Within the context of a model timestep, after the application of moist-convection, there usually follows the effect of stable-precipitation which precipitate by condensation any moisture in excess of saturation. This latter process is not included in this study since we concentrate on the effect of moist-convective parameterization schemes only in order to better isolate their behavior without interactions with other dynamical or physical components normally present in the model.

The observation operator H links the state-vector with the convective instantaneous precipitation-rate observations. This operator H is in general a composition of two operators:

$$H = \mathbf{F}\, C \quad .$$

Depending on the type of moist-convective scheme considered, C may be composed itself of more than strictly vertical operators acting on the state-vector. We define the vector of changes

$$\Delta \mathbf{x} = C(\mathbf{x}) \quad ,$$

where

$$\Delta \mathbf{x} = (\Delta \mathbf{T}, \Delta \mathbf{q})^T \quad ,$$

the heating and moistening in the column due to the convective scheme.

The linear operator $\mathbf{F}$ is such that

$$y = \mathbf{F}\, \Delta \mathbf{x} \quad ,$$

and is obtained from a discretization of the equation

$$y = \frac{p^*}{g\, \Delta t} \int_{\sigma_t}^{\sigma_b} \frac{c_p\, \Delta T}{L} d\sigma \quad (Kg\, m^{-2} s^{-1}) \quad ,$$

where "y" is the estimated observation value of the instantaneous precipitation-rate to be compared with the observation value "y^o", and the lower index b and t refer to the bottom and top of the cloud respectively. The analysis vertical coordinate is $\sigma = (p - p_t) / p^*$, $p^* = p_s - p_t$, with p pressure, p_s surface pressure, and p_t a prescribed, x,y-independent, top pressure. This is compatible with the geometry of the Mesoscale Adjoint Modelling System (MAMS, version 1) developed by Errico et al. (1994) used in this study. More details about the geometry of MAMS1 can be found in Section 5.

For SSM/I instruments, we could in principle use instead of the retrieval algorithms for rain-rate, an additional operator linking the model-state to the truly observed data (radiances for satellite data, Phalippou 1995, or reflectivity for radar data for instance). This additional step is not considered in the present study.

The convective operators based on parameterization of moist-convection are basically nonlinear and may also be non-differentiable for certain values of the state-vector. For the purposes of examining points (1) - (5) of Section 1, we consider only *non-pathological* convective regimes (i.e. convection always active during the minimization process) and assume that the observation operator is linearizable in the region D of significant posterior probability density in model-space (Tarantola 1987, ch I); i.e.,

$$\mathbf{H}_{\mathbf{n}}^{ik} = \left(\frac{\partial H^i}{\partial \mathrm{x}^k} \right)_{\mathbf{x}_n} \quad exists \ \forall \ \mathbf{x}_n \in D \quad ,$$

$$where \quad H = \mathbf{F}\, C \quad and \quad 1 \le k \le N \ .$$

Since the operator $\mathbf{F}$ is independent of $\mathbf{x}$, we have

$$\left(\frac{\partial H}{\partial \mathrm{x}} \right) = \mathbf{F} \frac{\partial C}{\partial \mathrm{x}} \equiv \mathbf{F}\,\mathbf{K} \quad ,$$

where $\mathbf{K}$ is a tangent-linear convective operator. Linearization aspects are further discussed in Sec. 5 for the two specific moist-convective parameterization schemes.

The gradient of J($\mathbf{x}$) at $\mathbf{x} = \mathbf{x}_n$, is

$$\frac{\partial J}{\partial \mathbf{x}_n} = \mathbf{H}_n^T \, \mathrm{R}^{-1} [H(\mathbf{x}_n) - \mathrm{y}^o] + \mathbf{B}^{-1} [\mathbf{x}_n - \mathbf{x}^b] \qquad (2)$$

where $\mathbf{H}^{\mathrm{T}}$ is the transpose operator of $\mathbf{H}$ given by

$$\mathbf{H}^T = (\mathbf{F}\,\mathbf{K})^T = \mathbf{K}^T \, \mathbf{F}^T \quad .$$

$\mathbf{K}^{\mathrm{T}}$ is hereafter referred to as the transpose (or adjoint) of the tangent-linear operator $\mathbf{K}$. The value of the functional J and its gradient as given respectively by (1) and (2) are passed to the "variable-storage quasi-Newton" module M1QN3 for unconstrained minimization provided by "Institut National de Recherche en Informatique Appliquée" (INRIA, France) (ref. Gilbert and Lemaréchal, 1989).

Due to the physical nature of the problem, the values of the total (analyzed) specific-humidity field must be such such that

$$0 \le q\big|_k \le q_{sat}\big|_k \qquad \forall \ k : \ 1 \le k \le N_k \qquad (3)$$

In general, an unconstrained minimum of J will be sufficient for most convective points (as discussed in section 5) but some points may lead the minimization to cross *infeasible* regions (i.e. regions where (3) is violated). In a similar way as was done with the problem of discontinuous convective transitions governed by the *conditionals* inherent to each convective schemes, we

avoided the use of the constraint (3) here since we are primarily interested in examining the natural occurence and degree of supersaturation states together with their effects on the minimization process. The study of these aspects will help elucidate the need to consider saturation constraints within a more complex variational framework that includes stable precipitation and different moist-convective schemes used. Different approaches are possible for the treatment of such non-linear constraints as (3), such as the *augmented Lagrangian function method* (Gill, Murray, and Wright 1981). The lower bound where the final q analysis must be non-negative was not found to represent a problem (this is confirmed in Section 5) due to the fact that the background term (via the error variances appropriate at each vertical levels) controls the amplitude of the changes made on specific-humidity, and also that very little moisture changes are made by the convective parameterization scheme at the upper levels where q is close to zero. The alternate choice of ln q as analysis variable was thus not necessary for this purpose. We now describe the convective schemes used for the minimization experiments.

3. Tangent-linear and adjoint of the moist-convective schemes

In this section we describe the approach taken to construct the tangent-linear (TL) and adjoint operators for the Kuo and RAS schemes respectively.

a. The Kuo-Anthes scheme

This scheme has the virtue of being very simple and still represents some basic effects that are useful to examine in the present 1D-Var context. The amount of convection in this convective parameterization scheme is determined by the vertically integrated moisture convergence. The feedback to the larger scales (the vertical distribution of heating and moistening), is represented with normalized vertical profiles of convective heating $N_h(\sigma)$ and moistening $N_m(\sigma)$. In addition, a vertical eddy-flux divergence of water vapor asssociated with cumulus convection is normally included in the nonlinear model but this effect in the model prognostic equation for moisture is discarded here.

The resulting heating and moistening due to moist-convection are given respectively by

$$\Delta T = \frac{L_v}{c_{p_d}} (1-b) Q_{ac} N_h(\sigma) \qquad (3.1)$$

$$\Delta q = b Q_{ac} N_m(\sigma) \qquad (3.2)$$

$$N_m(\sigma) = \frac{(1 - RH(\sigma))\, q_s(\sigma)}{\int_{\sigma_t}^{1} (1 - RH(\sigma))\, q_s(\sigma)\, d\sigma} \qquad (3.3)$$

where L_v and c_{pd} have their usual thermodynamic definitions. The normalized vertical heating profile $N_h(\sigma)$ assumes a simple parabolic shape in the vertical coordinate σ with a maximum in the upper half of the cloud, and vanishes outside the cloud (Anthes et al. 1987). For the present study, the 1D-Var scheme developed here makes use of fixed surface-pressure and *moisture-accession* Q_{ac}, and takes the form

$$Q_{ac} = -g^{-1} m^2 \int_0^1 \nabla \cdot \left(\frac{p^* \mathbf{V} q}{m} \right) d\sigma \quad ,$$

where "m" is Lambert's conformal map-scale factor.

The surface moisture flux is not considered in this approximation for Q_{ac}. The moisture partition parameter b (i.e., the fraction of Q_{ac} which is used to moisten the column) is given by

$$b = 2(1 - \overline{RH}) \quad ; \quad \overline{RH} \geq 0.5 \qquad (3.4)$$
$$1 \quad ; \quad \overline{RH} < 0.5$$

A vertical "mean" relative-humidity is calculated as

$$\overline{RH} = \int_0^1 q\, d\sigma \Big/ \int_0^1 q_s\, d\sigma \quad ,$$

where q_S is the saturation q at temperature T.

The sequence of equations involved in the construction of the tangent-linear system about basic-state profiles of T and q are

a. the solution of the Clausius-Claperon equation for the saturation vapor pressure given by

$$e_s(T_k) = 0.6112 \exp\left[\frac{17.67(T_k - 273.15)}{(T_k - 29.65)} \right]$$

b.

$$q_{s_k} = \frac{0.622\, e_s(T_k)}{p_k - e_s(T_k)}$$

c.

$$(RH)_k = \frac{q_k}{q_{s_k}}$$

d. Equation (3.3) for $N_m(\sigma)$.

e. Equation (3.4) for the moisture parameter b.

f. Equations (3.1) and (3.2).

No perturbations of p^* is considered. In addition, a *perturbation approach* was coded to compute the Jacobian matrix. The derivatives which appear as elements of the Jacobian are approximated using finite differences computed by repeated calls to the moist-convective scheme. The moist convective parameterization scheme may be considered as a one-dimensional nonlinear operator, designated C. The input to C is the state vector $\mathbf{x}$ and its output is the vector of changes $\xi = \Delta\mathbf{x}$ (ref. section 2). These vectors are of dimension $2N_k$ and the Jacobian matrix of elements of ξ with respect to those of $\mathbf{x}$ is $2N_k$ x $2N_k$. Each column of the Jacobian matrix is computed by determining the perturbations of ξ due to the perturbation of a single element of $\mathbf{x}$. The Jacobian matrix entries $c_{m,n}$ are then determined as

$$c_{m,n} = \frac{\delta\xi_m}{\delta x_n} \quad ,$$

where δx_n is the perturbation introduced and $\delta\xi_m$ is the m-th component of

$$\delta\xi = C(\bar{\mathbf{x}} + \delta\mathbf{x}) - C(\bar{\mathbf{x}}) \quad ,$$

where the overbar denotes a basic-state field.

There are $2N_k$ such computations required at each iterations of the minimization process in order to compute the gradient of the cost-functional. The amplitude of the perturbations introduced are respectively 10^{-4} degree for the temperature field and 10^{-3} g/Kg for specific-humidity. These amplitudes were determined by a careful examination of the accuracy of this perturbation method with the results obtained with the exact TL scheme available for this scheme. Many different

points were used to ensure the robustness of this choice of amplitude of the perturbations. The adjoint simply considers the transpose of the Jacobian matrix. Moreover, we ensured that the minimization behavior at these convective points produced identical results for both methods.

The "gradient-test" (see next section) was also verified for both methods. The same type of conditionals (i.e., convective criteria) as in the nonlinear Kuo scheme are computed in both the tangent-linear and adjoint code based on the profiles of T and q at the current iteration of the minimization process. These are summarized as:

(a) Check whether $Q_{ac} \geq critical\, Q_{ac}$

(b) Check for convective instability. This is obtained by calculating the equivalent potential-temperature Θ_e at all levels between 700 hPa and the surface, assuming that the parcel is 1^o K warmer and 1 g kg^{-1} moister than the environment at the same level. The maximum parcel Θ_e is then used as the Θ_e of the cloud base and defined as Θ_{ec}.

(c) Determine cloud-base from the computed lifting condensation level. The σ-level immediately below σ_{LCL} is considered to be the cloud-base level σ_{BASE}.

(d) Compute the saturation equivalent potential temperature Θ_{es} at all levels above σ_{BASE}. When the first level is reached at which $\Theta_{es} \geq \Theta_{ec} + \delta\Theta_e$ (where $\delta\Theta_e$ is included to allow for overshooting of convection, 3^oK here) the cloud-top is reached.

(e) If the cloud depth is less than a critical value (0.3 in σ-coordinates), then convection is not allowed.

(f) Check for positive "available buoyant energy" (ABE); i.e.,

$$ABE = \int_{\sigma_t}^{\sigma_b} (\Theta_{ec} - \Theta_{es}(\sigma))\, d\sigma \quad .$$

There are no conditionals related to the sign of the vertical motion or moisture convergence in the column as used in most current implementations of Kuo schemes. Neither is the effect of evaporation of the falling precipitation included here.

b. Relaxed Arakawa-Schubert scheme

Following Moorthi and Suarez (1992), we briefly give here the essential features of the RAS scheme and more details about this scheme and its impact in particuliar in the ARIES GCM at Goddard Laboratory for Atmospheres can be found in their paper.

the cloud model: 1- each cloud type is identified by its detrainment level (cloud top), 2- all clouds are assumed to have the same base, 3- the normalized mass-flux for each cloud type is a linear function of height, 4- the vertical coordinate is specified by the pressure at half-integer levels.

The Arakawa-Schubert closure assumption is a balance between large-scale and grid-scale effects on the cloud work function. The latter is a measure of efficiency of convection since it represents a kinetic energy generation per unit cloud mass-flux. In RAS, this quasi-equillibrium is also assumed but this is done by having each cloud act to relax the cloud work function to a prescribed value with a cloud-type-dependent time scale. Thus, the interaction between clouds occur over a short but finite time and at any instant each cloud (and each cloud type) feels only the "current" environment (i.e., the environment resulting from the effect of the previous cloud-type in the sequence of clouds treated at a given model time step). The effect of evaporation of the falling precipitation *is* considered here.

No explicit linearization of the RAS scheme was done. Instead, a perturbation method is used to estimate the Jacobian matrix. The same perturbation amplitudes on the temperature and specific-humidity fields as with the perturbation method for the Kuo scheme were used. The explicit TL scheme for the RAS scheme would be less expensive to use than the perturbation approach but was not considered for the purposes of the present study.

4. Numerical set-up

We describe in the following the procedure chosen to specify the background fields, the observations, and their respective error statistics together with the basic numerical aspects involved in the set-up of the minimization algorithm.

a. Background fields

The geometry of the problem (computational grid and operators) is based on MAMS1. The background fields used in the 1D-Var analysis were produced from a 12-h initialized forecast starting at 00UTC 12 February 1982 with a horizontal resolution of 120 km and 10 equally spaced sigma levels starting at $\sigma = 0.1$. There are 46 X 61 grid points in the north-south and east-west directions respectively. The moist-convective parameterization scheme used to produce the 12-h forecast was the RAS scheme. This rapidly developing meteorological case was also used by Ehrendorfer and Errico (1995) to study mesoscale predictibility using MAMS1 as a diagnostic tool. Figure 1 gives the location of convective points for both the Kuo (circles) and RAS schemes (cross marks). There are 234 convective points for the Kuo scheme and 411 points for the RAS scheme. The majority of Kuo convective points are located within regions where convergence of moisture occurs (i.e. troughs) and both schemes exhibits convective points in the frontal regions. The RAS scheme also exhibits more widespread convection in the tropics as compared to the Kuo scheme. It should be noted that the clear delimitation of convective points close to the boundaries is due to the absence of convective treatments of points within the sponge layers, which is restricted to the 5 nearest points from the model's boundaries.

b. Specification of a-priori error statistics

Since present knowledge about background-error statistics over convective areas is poorly (if at all) known, and the fact that we are primarily interested in the impact of varying the "correlation-scale" for both T and q fields, we follow the simple approach described in the following.

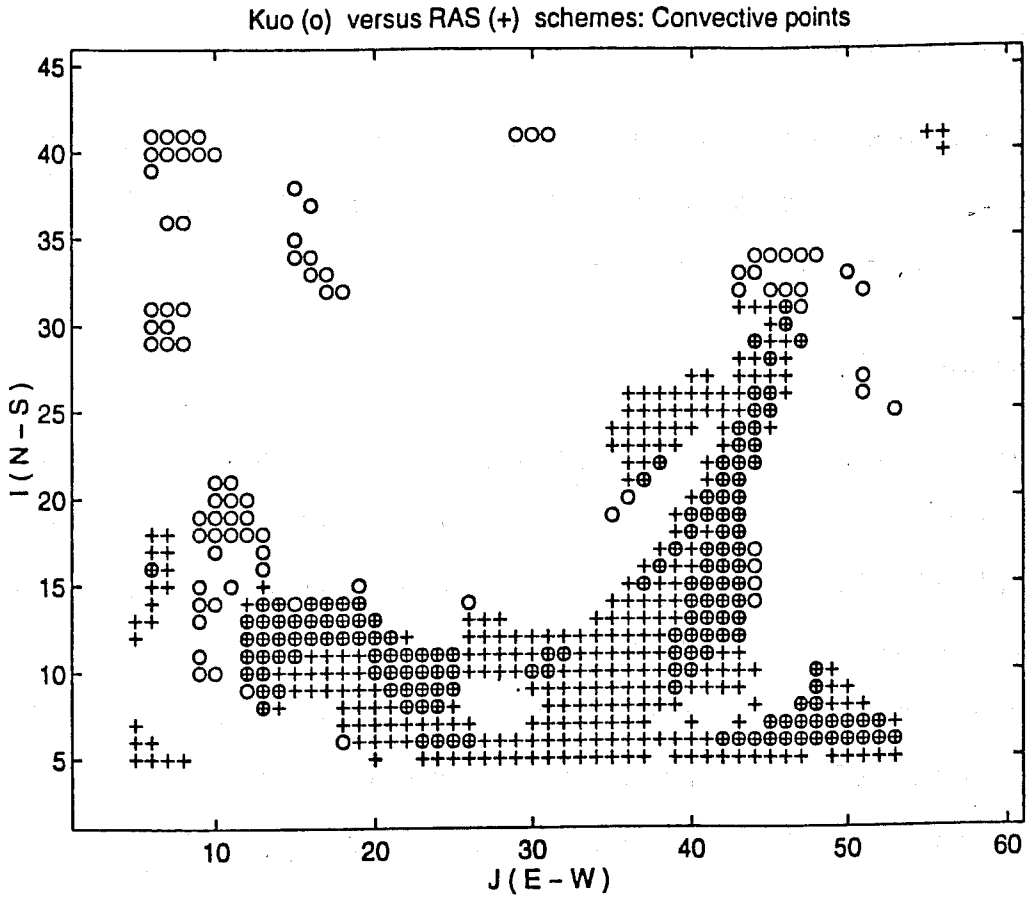

Fig. 1. Location of convective points for the Kuo-Anthes scheme (circles) and the RAS scheme (cross).

A Gaussian auto-correlation model is used for both temperature and specific-humidity fields; i.e.,

$$\rho_{ij} = \exp\left[-\frac{(\sigma_i - \sigma_j)^2}{2L^2}\right] \quad ,$$

where the scale-length L can be assigned differently for each fields. Due to a lack of a reasonable knowledge of the amplitude of the cross-correlations between T and q, these were neglected. The background-error variances are allowed to vary in the vertical for both fields. Some experiments to be described later in the text will make use of profiles of background-error variances for temperature, deduced from an old version of the Canadian operational OI analysis scheme. These statistics were in use operationally until September 1994. Regarding the standard-deviation of the background error for specific humidity, the operational OI scheme has the dew-point depression as

an analysis variable instead of specific humidity. The required statistic was instead extracted from Table 3a of Deblonde et al (1995) and corresponds to 6-h forecast-error statistics for the Northern-Hemisphere between 30° - 60° N done with the Canadian Meteorological Center (CMC) global spectral semi-Lagrangian model where a triangular 79-wave truncation was used operationally at the time (ref. Ritchie 1991). The vertical structure of this latter statistic compares reasonably well with other studies such as in Norquist and Chang (1994). Table 1 shows these statistics for T and q fields respectively for each half-sigma levels of the staggered grid used for the analysis. These staggered levels are being used also by the model in MAMS1. Note that the error for the specific-humidity field was kept constant above 300 hPa.

Half-sigma level:	0.05	0.15	0.25	0.35	0.45	0.55	0.65	0.75	0.85	0.95
Temperature (deg):	1.2	1.5	1.3	1.4	1.3	1.4	1.4	1.6	1.7	2.5
Specific Humidity (g/Kg):	0.04	0.04	0.04	0.12	0.24	0.32	0.52	0.71	0.78	0.92

Table 1. Background-error standard deviations on analysis levels

c. Specification of data and data-error statistics

Rain-rate "observations" are being simulated as we wish to give the flexibility to examine various minimization aspects related to the amplitude of the innovation (observation increment) at a given convective point. These values are given as we describe the experiments in Section 5. Concerning the specification of the standard-deviation error for the "observed" instantaneous precipitation-rate σ_p, we have the flexibility to examine its effect on the minimization and resulting analysis. Present knowledge about realistic error specification of this type (e.g. Garand and

Grassoti, 1995), where the estimated σ_p can be *categorized* according to the intensity of precipitation, indicates that this statistic can be as high as the background precipitation-rate itself for weak precipitation cases. Since various estimate of σ_p from most instruments giving instantaneous precipitation-rate estimates (e.g. SSM/I retrieval algorithms, radars, surface gauges) or indirect inference procedures (e.g. geostationary satellite imagery as in Grassoti and Garand, 1994) will reasonably fall in this realistic range of σ_p less than the background precipitation-rate, the effect of this order of variation on σ_p will be examined in Section 5.

d. Control variable and preliminary tests

The control variable for the minimization is defined as follows. Due to the low-dimensional minimization problem involved (20 here), it is an easy task to exploit the eigenstructure of the background-error covariance matrix **B**. By definition, **B** can be diagonalized as

$$\mathbf{B} = \mathbf{E}\,\Lambda\,\mathbf{E}^{-1} \quad ,$$

where $\mathbf{E}$ is the matrix whose columns are the eigenvectors $\mathbf{e}_n$ of **B**, $\mathbf{E}^T$ is the transpose of $\mathbf{E}$, and Λ is the diagonal matrix of eigenvalues λ_n. Since **B** is real and symmetric, the columns of $\mathbf{E}$ are orthogonal, $\mathbf{E}^T = \mathbf{E}^{-1}$, and the eigenvalues are all real. Defining the control variable (or preconditioned state variable) as

$$\mathbf{v} \equiv \Lambda^{-1/2}\,\mathbf{E}^T(\mathbf{x} - \mathbf{x}^b) \quad ,$$

with the inverse transform

$$\mathbf{x} = \mathbf{x}^b + \mathbf{E}\,\Lambda^{1/2}\,\mathbf{v} \quad ,$$

the background term becomes

$$J_b = \frac{1}{2}\,\mathbf{v}^T\,\mathbf{v} \quad .$$

The inverse transform and its adjoint are required for the evaluation of the observational term J_o. In accord with this change of variable, a Euclidean scalar-product is initialized and passed to the minimization algorithm. Such a change of variable improves the conditioning over the original variable **x**. For minimization of J_b alone, only one iteration is thus necessary. The observational term J_o of course renders less "optimal" the above preconditioning procedure.

Second, as discussed in the previous section, the gradient of the functional requires the adjoint operators $\mathbf{K}^{\mathrm{T}}$ and $\mathbf{F}^{\mathrm{T}}$. Using a Euclidean inner product, Lagrange's identity was verified for both operators at basic-state points where convection exists. First, verify

$$\left\langle \mathbf{K}_{\mathbf{x}_1}\, \delta\mathbf{x}_1,\ \delta(\Delta\mathbf{x})_2 \right\rangle = \left\langle \delta\mathbf{x}_1,\ \mathbf{K}_{\mathbf{x}_1}^{\mathrm{T}}\, \delta(\Delta\mathbf{x})_2 \right\rangle \quad ,$$

where $\delta(\Delta\mathbf{x})_2 = (\ \delta(\Delta\mathbf{T}),\ \delta(\Delta\mathbf{q})\ )_2^{\mathrm{T}}$, was specified by applying the tangent-linear operator at the *convective* point $\mathbf{x}_2$. The subscript $\mathbf{x}$ for the operators means that this operator is computed with $\mathbf{x}$ as basic-state. Also, it was simply verified that

$$\left\langle \mathbf{F}\,\delta(\Delta\mathbf{x}),\ \mathbf{y} \right\rangle = \left\langle \delta(\Delta\mathbf{x}),\ \mathbf{F}^{\mathrm{T}}\mathbf{y} \right\rangle \quad .$$

The "gradient test" was also performed at representative convective points (defined in Section 5) common to the Kuo and RAS schemes. For both schemes, we verified that

$$\lim_{\alpha\to 0} r \;=\; \lim_{\alpha\to 0} \frac{J(\mathbf{x} + \alpha\,\mathbf{grad}\,J) - J(\mathbf{x})}{\left\langle \mathbf{grad}\,J,\ \alpha\,\mathbf{grad}\,J \right\rangle} \;=\; 1 \quad ,$$

where the residual of r approaches zero linearly. We now proceed to examine the results of the 1D-Var scheme.

5. Results

a. Selection of profiles

We have examined the intersection ensemble of Kuo and RAS convective points (149 points) and selected 4 convective points which typically represent the essential features of interest for the present study. The grid-coordinates (I, J) of these points are: (10, 12), (24, 43), (19, 41), and (20, 43), hereafter referred respectively as points 1 to 4. We present in Fig. 2 the vertical profiles of relative-humidity for these four points. Figure 3 shows the associated heating-rates (K/day) for the Kuo scheme (solid line) and the RAS scheme (dashed-line) at these four points. The point 1 lies in the deep but weak convective region over the Gulf of Mexico where both convective schemes agree relatively well on the intensity of convection. The lowest layers are

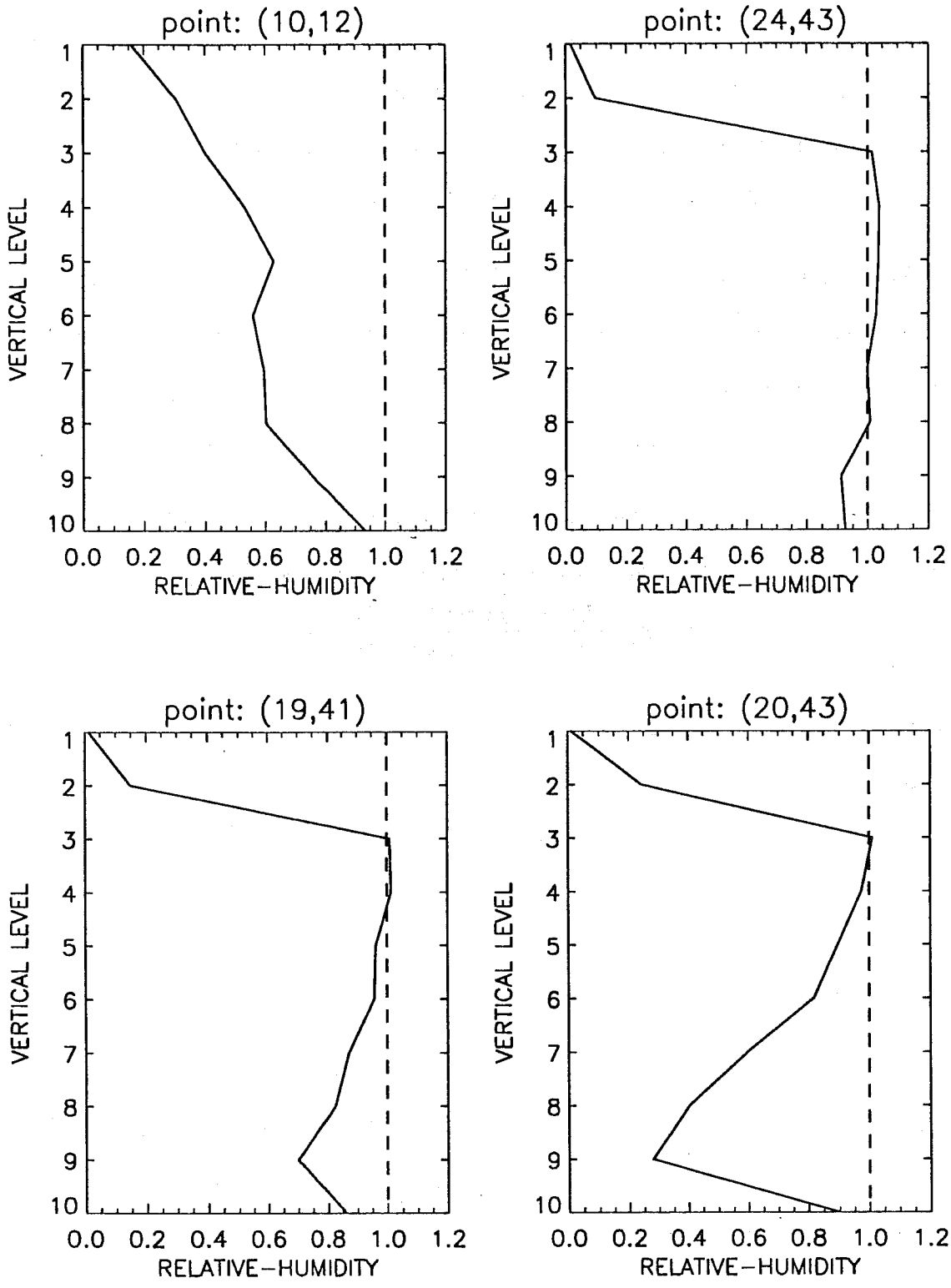

Fig. 2. Vertical structure of the relative-humidity field for four typical convective points used to examine the 1D-Var minimization.

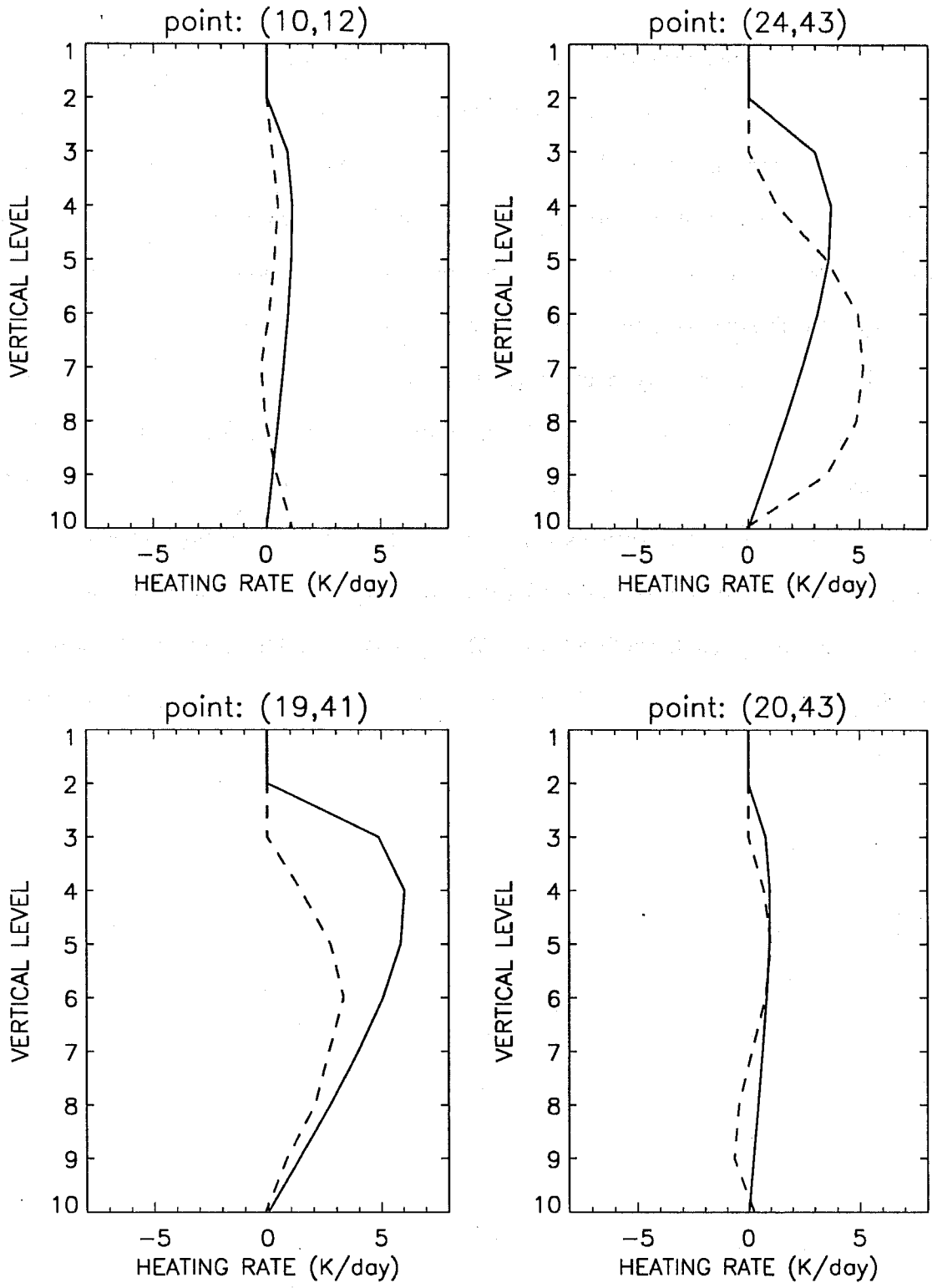

Fig. 3. Heating-rate response of both convective schemes for the same four points as in Fig. 2. The solid line is for the Kuo-Anthes scheme and the dashed line is for the RAS scheme.

close to saturation. The Kuo scheme used here uses the Anthes et al. (1987) approximation of parabolic vertical profile of heating-rate within the cloud region. Also, the RAS scheme as used here always assumes the base of the cloud to be at the lowest model-level. Point 4 represents also a weak convective regime located immediately on the east-side of the cold front associated with the low-pressure system of the east-coast but was chosen in addition to point 1 for its typical vertical structure frequently observed with the RAS scheme under weak convective activity. As can be seen in Fig. 2, point 1 has its lowest layers close to saturation whereas point 4 is close to saturation at the highest layers. In addition to these weak convective regimes, Fig. 3 presents points 2 and 3 where convection is significant in both schemes (the RAS scheme having its maximum heating at the lowest levels whereas the Kuo-Anthes scheme places the maximum heating in the upper part of the convective layer). Point 3 shows a relatively good agreement in intensity and a vertical localisation of the heating-rate for both schemes. Both points 2 and 3 have a vertical distribution of moisture which is close to saturation and we examine the impact of this in the minimization results of sub-section (e).

c. Sensitivity of convection

Figure 4 shows the four components of the Jacobian matrix for the Kuo scheme for the convective point 3. Both the perturbation and explicit tangent-linear approaches were compared to make sure the amplitude of the perturbations on T and q using the finite-difference method was within the range of accuracy of the exact TL scheme available for the Kuo scheme constructed from a linearization of the nonlinear Kuo scheme. Figure 5 shows the same four components of the Jacobian for the RAS scheme for the same convective point as Fig. 4 where a perturbative approach was used to compute the Jacobian using the same order of magnitude perturbations as used with the Kuo scheme. It is interesting to note that due to the special form of the Kuo-Anthes scheme used here, the sensitivity of the heating-rate also reflects the sensitivity of the partition parameter "b".

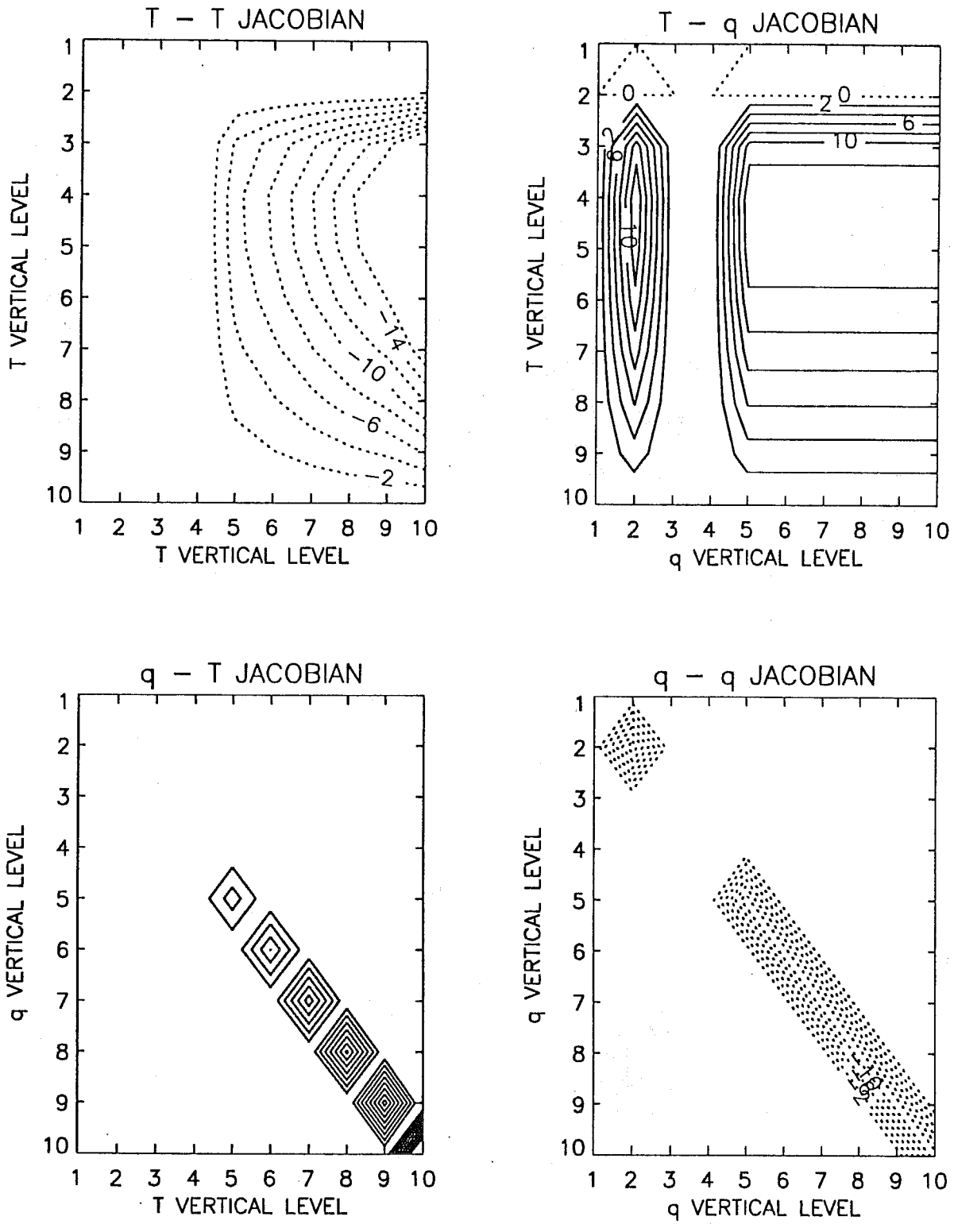

Fig. 4. The four blocs of the Jacobian matrix obtained by perturbing the background temperature and specific-humidity fields. The T-T panel is for the variation of the *heating-rate* at various vertical levels to perturbations of the *temperature* field at different levels. The other panels have similar interpretations. The Kuo-Anthes scheme was used. Scaling factors 5 x 10^3, 2.0, 2 x 10^6, and 10^3 were applied to the T-T, T-q, q-T, q-q Jacobians respectively.

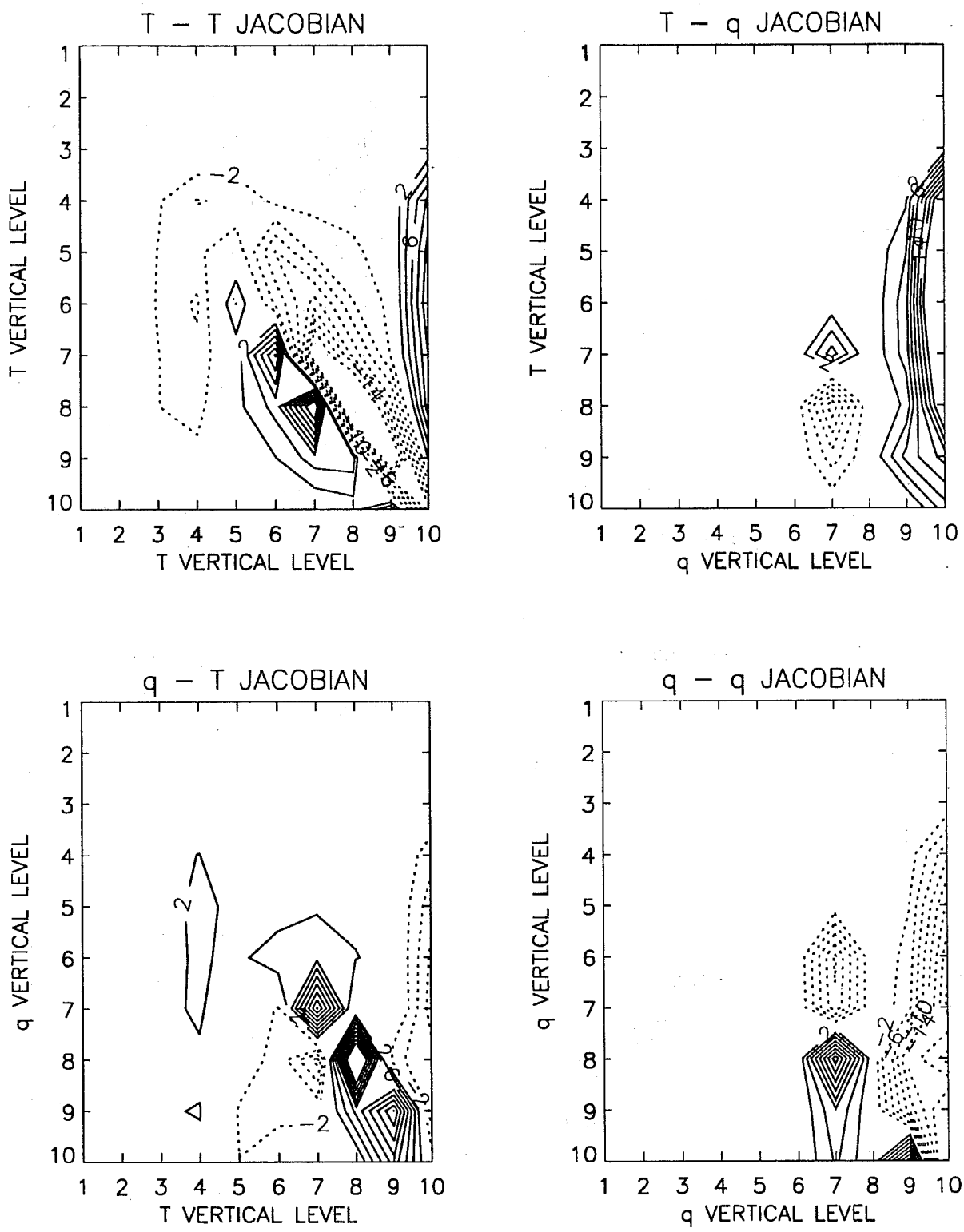

Fig. 5. Same as in Fig. 4 but for the RAS scheme. Scaling factors 5 x 10^2, 0.5, 10^6, and 10^3 were applied to the T-T, T-q, q-T, q-q Jacobians respectively.

An interpretation of the T-T sensitivity can be given using convective stability arguments. As can be shown using results from the RAS scheme for instance, increasing the temperature at level 10 (the model's lowest level) increases the heating-rate due to convection from level 8 to the top of the convective cloud. On the other hand, increasing the temperature at level 9 or in the cloud above, tends to stabilize the column and so decreases the amplitude of convection; i.e., heating-rate. As will be apparent later when discussing minimization experiments, the Kuo scheme appears to achieve an increase in the amount of heating by systematically lowering T for all vertical levels whereas the RAS scheme exhibits a more complex vertical structure where both lowering of T at some levels or increasing T at other levels are ways to increase the heating-rates at these levels. A marked difference also exists between the two convective schemes with respect to the T-q Jacobian. The RAS scheme exhibits a strong upper-level "diagonal" structure which was systematic for all convective points examined. The increased heating-rate throughtout the whole convective column due to an increase of q at the lowest levels 9 and 10 was also systematic. On the other hand, the Kuo scheme exhibits the same sensitivity for all levels from the cloud base to level 5 and at cloud top (level 2), and the sensitivity starts to be purely "barotropic" for perturbations in the vicinity of the maximum heating-rate. This response indicates that the perturbation levels where a *minimum* increase in heating-rate can be achieved for a definite increase of moisture appears at levels where the Kuo scheme produces a *maximum* heating-rate from the background fields. A zero contour line was added here to make clear that the minimum sensitivity just discussed for levels 3 and 4 was not zero but around a value of 2 (normalized units).

Finally, the q-T and q-q sensitivity figures for both schemes exhibit a strong diagonal structure (localized effect on moistening due to convection), but as mentioned for T-T maps, the RAS scheme can produce drying (moistening) at the highest (lowest) levels in accordance with the heating-rate structure. The RAS scheme, for all components of the Jacobian, has a strong sensitivity to the very lowest layers. No further discussion is given to the q-T and q-q Jacobian blocks since the relevant parts of the Jacobian for the problem addressed here are those affecting the heating-rates; i.e., T-T and T-q components of the Jacobian.

d. Range of validity of tangent-linear schemes: Monte Carlo simulations

In order to assess the range of validity of the TL schemes for both Kuo and RAS schemes, a comparison is made between the result of TL schemes versus the difference between two nonlinear computations; i.e., we compare

$$\delta\xi = \mathbf{K}_x \, \delta\mathbf{x} \quad with \quad \Delta\xi = C(\mathbf{x} + \delta\mathbf{x}) - C(\mathbf{x}) \quad ,$$

for a given perturbation $\delta\mathbf{x} = (\delta T, \delta\mathbf{q})^T$. A large number of such perturbations were generated in order to get a robust indication of the range of validity of the TL schemes. The procedure to generate these perturbations uses the eigenvectors/eigenvalues of the background-error covariance marix **B**, thus covering a realistic region of phase-space where the TL schemes must be diagnosed. Each perturbation is represented as

$$\delta\mathbf{x} = \sum_{i=1}^{2N_k} g_i \sqrt{\lambda_i} \, \mathbf{e}_i \quad ,$$

where the g_i are random numbers Normally-distributed with zero mean and unit variance (i.e., N(0;1)). A scaling factor is applied to these perturbations and the nonlinear regime is examined by varying this scaling factor. Two quantities are computed; the standard-deviation of the differential nonlinear response (defined above), and the standard-deviation of the error of the TL scheme; i.e.,

$$\sqrt{\overline{[(\delta\xi - \Delta\xi) - \overline{(\delta\xi - \Delta\xi)}\,]^2}} \quad ,$$

where the overbar denotes an ensemble-mean.

In order to cover the ensemble of possible perturbation structures allowed with the **B** matrix, 10^3 simulations were used. With only 10^2 simulations, there remains significant differences in the reconstructed cross-correlations between T-q fields where these terms strictly vanish in the original correlation matrix. We stress here that only *non-pathological* perturbations (ref. Sec. 2) were used to examine the accuracy of TL schemes.

Figure 6 shows the two measures mentioned above computed at the convective point 2 for both RAS scheme (upper-panels) and the Kuo scheme (lower-panels) respectively. In each panel, the solid line refers to the standard-deviation of the signal (i.e., changes in the heating-rates)

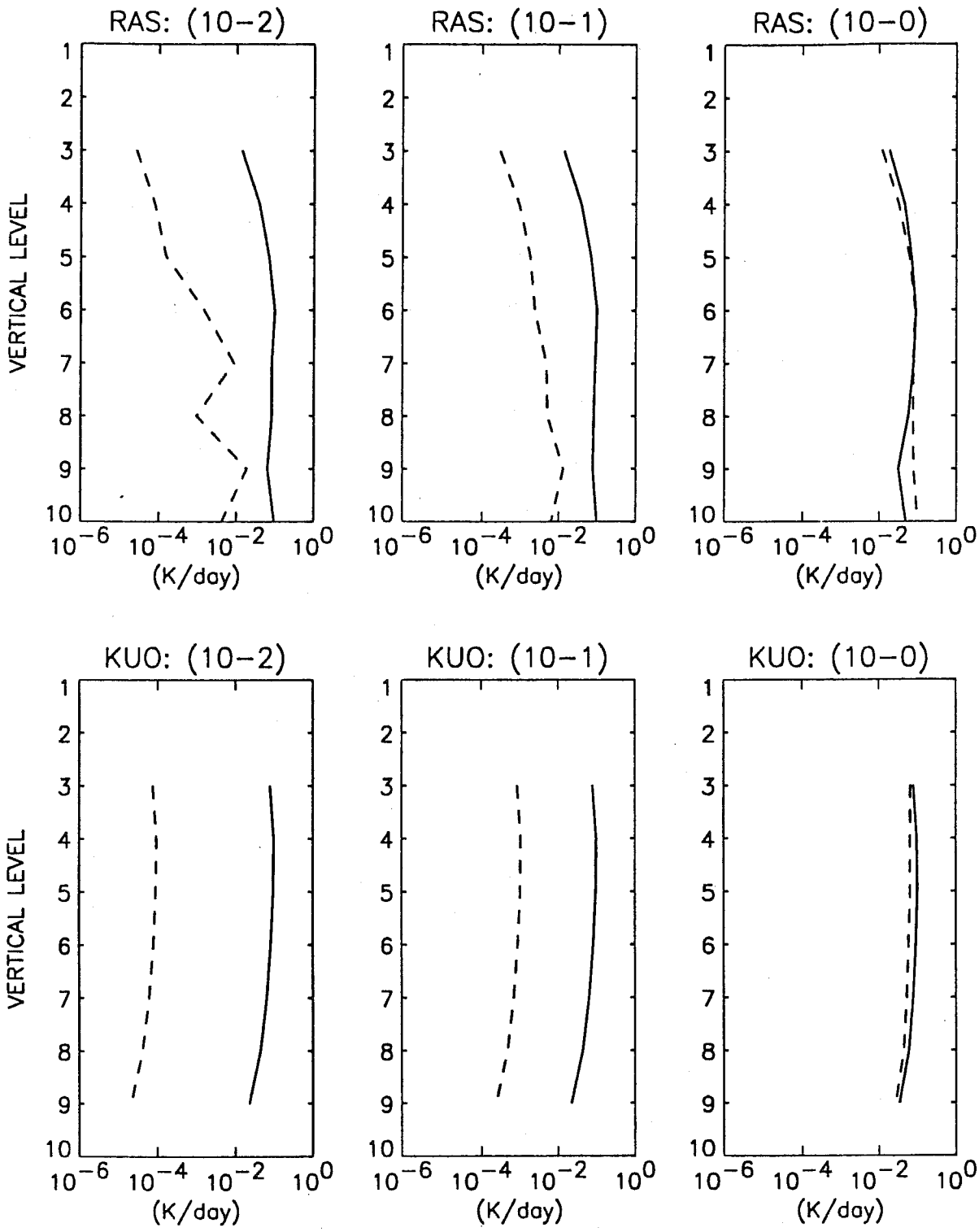

Fig. 6. Measure of nonlinearity. Upper panels: RAS scheme; Lower panels: Kuo scheme. Solid line: standard-deviation of the nonlinear differential heating-rate response. Dashed-line: standard-deviation of the error of the TL scheme. The amplitude factor on top of each panels is applied to the input perturbation structure and is varied from 0.01 to 1.

whereas the solid-line refers to the standard-deviation of the TL scheme error. The scaling factor on the perturbation vector is indicated on top of each panels and varies from 10^{-2} to 10^{0} with the latter indicating perturbation sizes as in Table 1. For graphical purposes, the two measure mentioned above are being rescaled before plotting to make the signal curve (solid-line) close to a value of unity on the abscissa and since the physical units for the quantity being measured refers to differences in heating-rates, units of K/day are being used. It is seen that with a scaling factor of 10^{-2}, the standard-deviation of the error for the RAS scheme is typically one order of magnitude smaller than the signal itself at cloud-levels between the cloud-base and level 7, and then about 2 orders of magnitude higher-up in the cloud. However, the TL of the Kuo scheme has a quite uniform accuracy in the vertical where the error is typically around 2 orders of magnitude smaller than the signal. Using a scaling factor of 10^{-1} reduces the accuracy of the TL for RAS scheme uniformly in the vertical to about one order of magnitude relative to the signal. The Kuo scheme has gone from an original 4 orders to 2 orders of accuracy uniformly in the vertical. Finally, when the scale factor is 1, both schemes exhibit the same magnitude errors being typically of the same order of magnitude as the signal at all vertical levels.

Moreover, in Fig. 6, in the RAS scheme the cloud-top is not allowed to be above 200 hPa which corresponds to level 3 as highest coud top. There is a degradation of TL accuracy at both cloud top and base for this scheme as shown in the upper panels (level 3 and 10 resp). For the Kuo scheme, because of Anthes's approximation (i.e. parabolic profile for the heating-rate), *by construction*, the normalized profile N_h is determined using *zero* boundary conditions at the top and base of the cloud. Thus, according to (3.1), the heating-rate at these boundaries is zero. This is the reason why the curves do not extend to level 2 and 10 (cloud top and base respectively of the basic-state profile) for the lower panels associated to Kuo scheme.

A similar behavior in the accuracy of the TL schemes was observed at many other convective points examined (results not shown). The conclusion from these results is that *for convective states examined (excluding pathological ones), we can expect that the part of the gradient of the functional which involves computation of the adjoint of the TL of the moist-*

convective parameterization scheme (i.e., the observational term as defined in Section 2) approximate the non-linear variation of the functional to about one to 10 % error for step-sizes along the gradient which are typically 10 % the size of the backgrond error standard-deviation. As we will see in the following sub-section, this represents grossly the largest typical orders of magnitude of changes on the temperature and specific-humidity encountered during the first few *iterations* of the 1D-Var minimizations.

e. Diagnostics of 1D-Var adjustments

Preliminary comments : Due to the special nature of the 1D-Var scheme, the direction taken by the two convective schemes during the minimization process when the attempt is made to increase the precipitation-rate, will be toward states *close to saturation.* In light of the basic mechanism characterizing the Kuo scheme, keeping the moisture accession fixed, the only varying parameter will be the partition parameter "b" (ref. eq. 3.1). This means that this parameter will be reduced or even set to its minimum value of zero during the minimization process depending on the amplitude of the innovation. In terms of (3.4), this means that we are going to face saturation.

Except when explicitly mentioned, the diagnostics to be presented are for minimization performed with sharp correlation scales of 0.1 for both temperature and specific-humidity fields. We demonstrate the impact of varying this scale at the end of this section. Experiments where the precipitation-rate is reduced instead of being increased lead to similar conclusions as those discussed below, except for the saturation problem which becomes less relevant. Finally, note that the value of the background precipitation-rate is available from the precipitation-rate panel at iteration zero.

Point 1: As mentioned in Section 4c, the estimated standard-deviation error σ_p for the observed precipitation-rate for such a weak precipitation case (initial value of 1 mm/day using the RAS scheme) may realistically be as large as the background precipitation-rate itself. We first discuss the result of using a value of σ_p = 25 % of the background precipitation-rate and then

further experiments where both the innovation and σ_p are increased. Figure 7a gives various measures of the behavior of the minimization *using the Kuo scheme.* First, we see that the norm of the gradient of the functional has been modestly reduced by one order of magnitude after which it exhibits a "oscillatory" type of behavior in the course of iterations. After 16 iterations, the minimization module was stopped (no minimization is active for values between 16 and 20, these values were held fixed in the figure for later comparisons).

As mentioned at the beginning of section 5, we are allowed to vary as we wish the value of the "observation" of the precipitation-rate and we used a 50 % increase from the background precipitation-rate which was (for this weak case) about 2.2 mm/day (Kuo scheme). The precipitation-rate of that analysis has been increased to 2.8 mm/day. Note that this value is reached after 2 to 3 iterations and only very small changes are being made before we enter in the oscillating regime appearing in the norm of the gradient which occurs after iteration 6. Also, Fig. 7a shows the behavior of the minimization with respect to temperature and specific-humidity changes as a function of iterations. Five curves appear on each frame starting with the value of the analysis increment obtained after iteration 3 (solid-line) to iteration 7 (long-dashed line). This applies to all the figures to be discussed in this section. The analysis increment for q exhibits regular convergence whereas for temperature it is also regular except at level 9 and 10. The "oscillating" behavior mentioned previously with the norm of the gradient is associated with too small changes on T and q to be perceptible in this figure and start to appear at iteration 6 (only analysis increments at iteration 3-7 are shown here). The source of the "oscillating" problem is shown in the last frame of Fig. 7a which shows the final relative-humidity of the analyzed state and it can be seen that level 10 reached saturation. The "oscillation" problem has an easy explanation.

Because values of q at the lowest levels largely dominate the effect of very small subsaturated values at the upper levels, the value of $\overline{RH}$ (as defined in Section 3a) from the background fields is close to 1. The minimization scheme attempts to move into non-feasible regions according to (3.4), resulting in values of $\overline{RH} > 1$. In the nonlinear Kuo scheme, a threshold value is applied at b = 0 (i.e., $\overline{RH} = 1$). The line of code $\overline{RH} = \min (\overline{RH}, 1)$ was

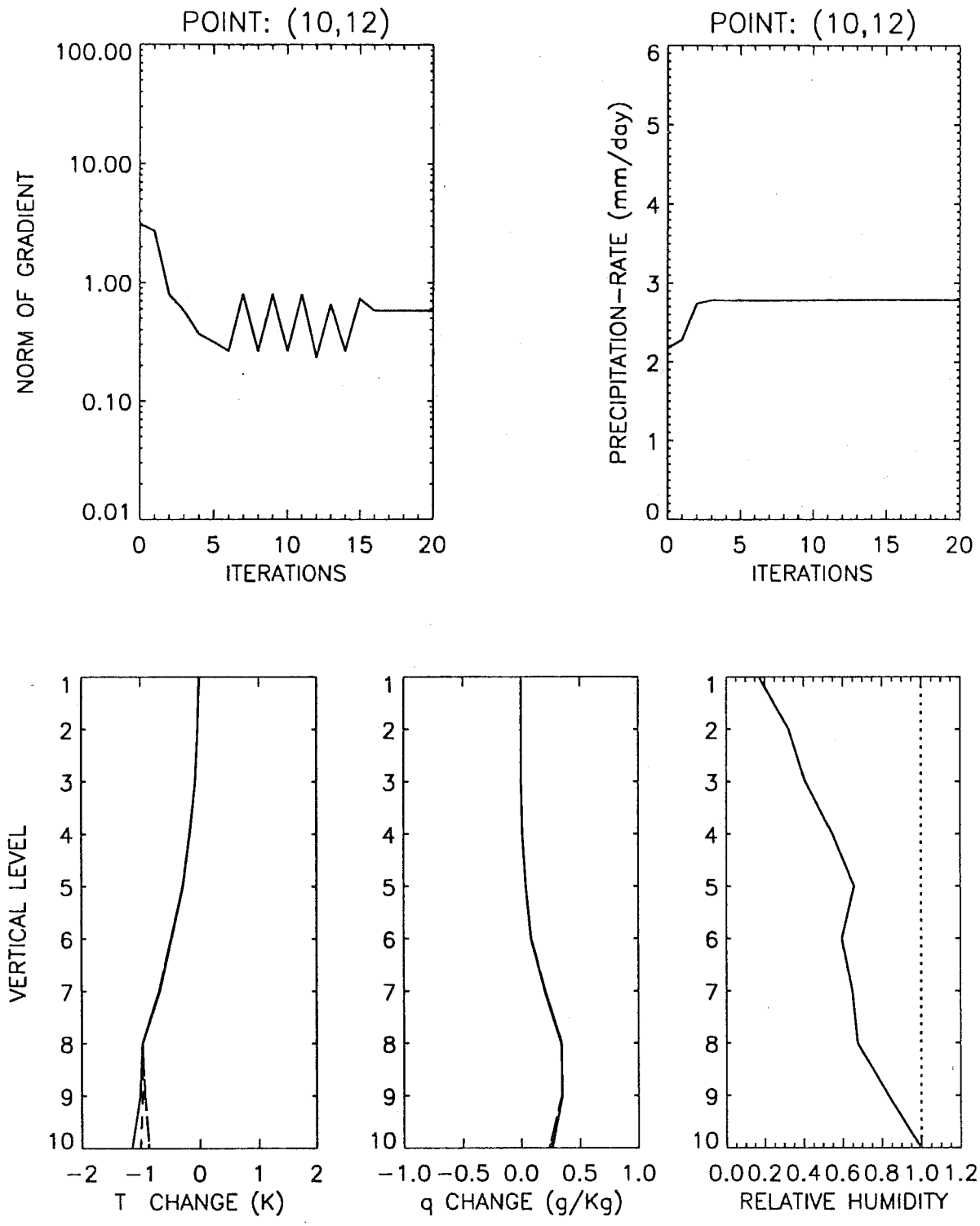

Fig. 7a. 1D-Var minimization for point 1 located at I-J grid-coordinates (10, 12) for the Kuo scheme. For the temperature and specific-humidity changes (i.e., analysis increments), the solid line is for the resulting profile at *iteration* 3 and the long-dashed curve is associated to iteration 7. The other curves are associated to the intermediate iterations of the minimization. The precipitation-rate observation is 50 % larger than the background value and the standard-deviation error for precipitation-rate observations was set to 25 % of the background value. The correlation scales for T and q are 0.1 for both fields.

removed and the experiment reran. That means that the partition parameter "b" is now allowed to be *negative* thus producing larger values of heating-rates and drying effect from convection according to (3.1) and (3.2). We present in Fig. 7b the same diagnostics as before, and it is clear that the "oscillating" problem in the norm of the gradient has disappeared and the norm of the gradient is reduced by about 7 orders of magnitude after 20 iterations and is monotonically decreasing. The final precipitation-rate is slightly larger than the previous case, and we see that the oscillation in the structure of the analysis increment at level 10 has disappeared. Note also that this has been achieved at the expense of producing supersaturation at that level as shown in the relative-humidity panel in Fig. 7b. The conclusion here is that *with the Kuo scheme, a "smoothing" procedure is required when* $\overline{RH}$ *gets close to the critical value of 1. This is also necessary when a few layers in the bottom of the model are close to saturation and very dry upper levels (as is the case here) since the background error on the temperature field is most significant at the lowest levels (ref. Table 1).* The modified Kuo scheme of Geleyn (1985) may possibly avoid this specific problem with the partition parameter since the latter parameter has essentially been removed from the problem and replaced by a more local (i.e vertically dependent) definition of the partition criteria.

Figure 7c shows the same type of diagnostics as Fig. 7a for the convective point 1 but with the RAS scheme. We see that the norm of the gradient has been reduced by 4-5 orders of magnitude after about 10 iterations. Note that since the convective scheme used here is different than the one used in Fig. 7a, the initial values of the norm of the gradient for both cases are different. Also, since we use a synthetic precipitation-rate observation specified as 50 % increase with respect to the background precipitation-rate, and the fact that each convective schemes produces its own heating-rate (which are different here) from the same background profiles of T and q, the initial values of precipitation-rates appearing in Fig. 7a and Fig. 7c are different. As for the Kuo scheme, the adjusted precipitation-rate is achieved after only 2-3 iterations. While the Kuo scheme produces analysis increments of T which are negative (cooling) and quasi-monotonically decreasing in the vertical, the RAS scheme essentially differs from this behavior at the lowest

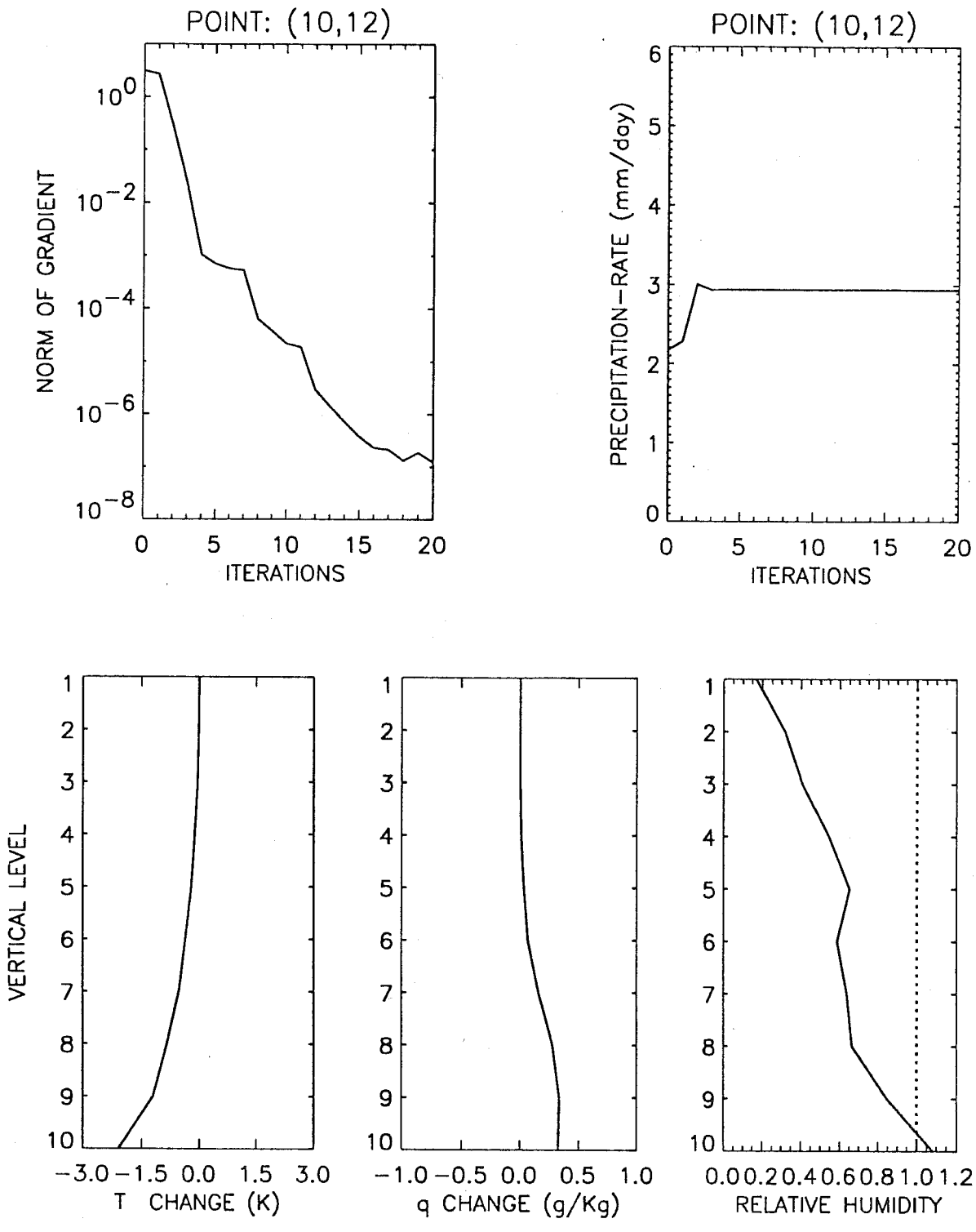

Fig. 7b. Same as in Fig. 7a but the "b" parameter is allowed to be negative.

layers where a negative vertical temperature gradient is achieved instead of a positive gradient for the Kuo scheme. Smaller changes to the specific-humidity field are also obtained for the RAS scheme. As in Fig. 7a, Fig. 7c shows the vertical profiles of T and q analysis increments valid after 3-7 iterations, and it is seen that these five curves are almost exactly superimposed. A two-order reduction in the norm of the gradient is achieved after only 2 iterations and appears sufficient. We note also from the relative-humidity panel in Fig. 7c that the RAS scheme has not saturated any levels in contrast to the Kuo scheme.

This must be compared with findings by Kasahara et al. (1996) where, the same computer code for the Kuo scheme and very similar code for the RAS scheme as those of the present study were used. They showed that their "inversion" scheme required only small moisture changes when the RAS scheme was used and that their final analyzed q field with the RAS scheme was far from saturation as compared to other convective schemes examined (see their Figs. 14 and 20 and their conclusion section). As we will see in the following, there is indeed indications of this in our 1D-Var context. It must be stressed however that important distinctions exists between the two approaches since their scheme adjusts only the specific-humidity field leaving the background temperature field fixed and they allow adjustment of the divergent part of the wind field (which affect the moisture accession) in an external iteration loop.

To give insight on the possible impact of varying the amplitude of the σ_p statistic for this convective point, we perform another minimization experiment using the RAS scheme but now with a value of σ_p as large as the background precipitation-rate itself in order to obtain a more realistic indication of the behavior of the scheme with real precipitation-rate data for such weak convective regimes. The analogous panels as those presented in Fig. 7c are not shown since the results are very similar in terms of the increase in precipitation-rate at the end of the minimization (around 2.5 mm/day) and the analysis increments on T and q, and the final analysis value of the relative-humidity. The decrease in the norm of the gradient is about 6 orders of magnitude after 18

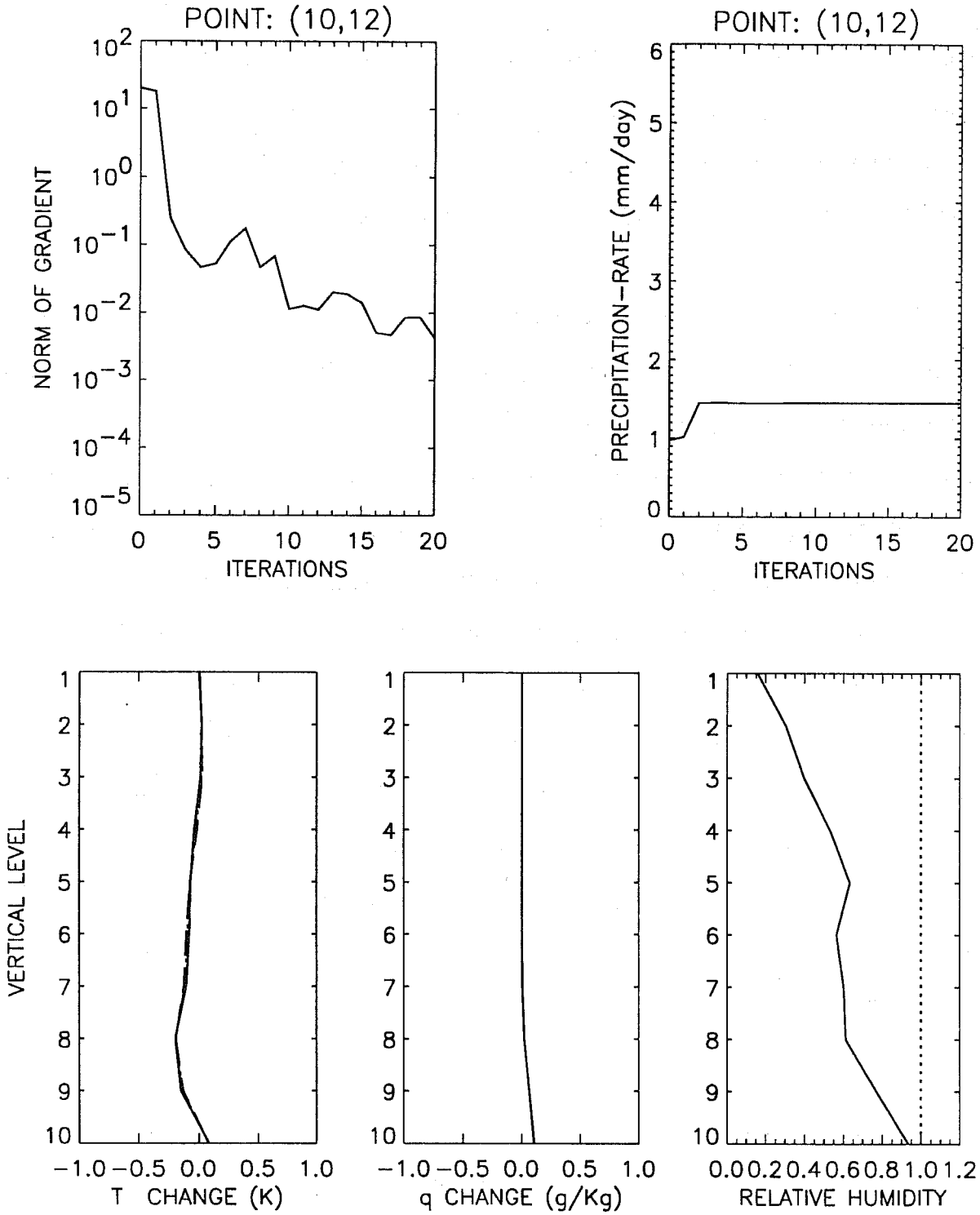

Fig. 7c. As in Fig. 7a but for the RAS scheme using a precipitation-rate observation larger than the background value by 50 %. The standard-deviation error for the observations σ_p was set to 25 % of the background precipitation rate.

iterations and is comparable to the behavior shown in Fig. 7c except that the initial value now is around a value of 1 (this is expected from the form of the observational term in (1) and the fact that the initial minimization point is the background state). It thus appears that under realistically large values of σ_p for weak convective regimes, the minimization remains well-behaved.

We now examine the effect of increasing the amplitude of the innovation using σ_p fixed to the value of the background precipitation-rate (i.e., realistic configuration). Previously, we used a precipitation-rate observation which represented a 50 % increase w.r.t. the background precipitation-rate, but now we increase it to 100 %. The results (not shown) are close to the aforementioned experiment except that now the precipitation-rate from the resulting analysis increased to a value of about 3 mm/day. We note that the possibility to increase the precipitation-rate is bounded from above due to the presence of the background term that precludes analysis increments on T and q of being significantly larger than the background-error for these fields. Experiments were continued by increasing the innovation up to a ratio of 3 times σ_p (which corresponds to a 300 % increase w.r.t. the background precipitation) and the results are presented in Fig. 7d. In the context of standard Quality Control tests, this would represent a limit of admissible innovations. We see in panels of T and q changes in Fig. 7d, that we are at the limit where the background term controls the changes to the background fields and we also note that level 10 approached saturation.

Such a large discrepancy between the observations and what the model produces as precipitation-rate from the background field may be expected when a significant phase-error exists between the precipitation area present in the model forecast and what the observation instrument sees. The RAS scheme appears to be particularly effective in increasing the precipitation-rate for such convective regimes. However, as we will see in the next experiments, we must be carefull with such attempts.

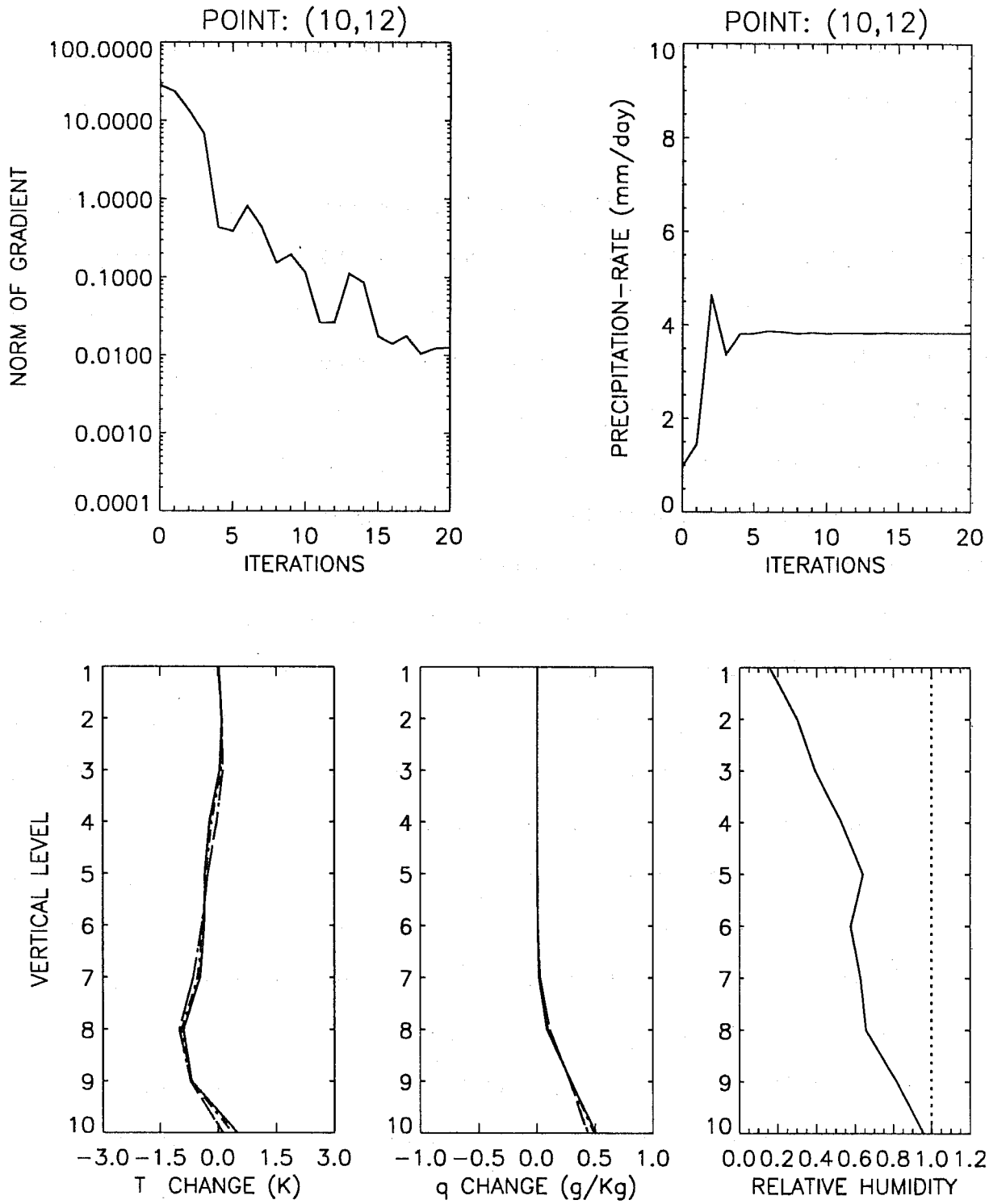

Fig. 7d. As in Fig. 7c except that σ_p was set to the value of the background precipitation-rate. The precipitation-rate observation was set so that the innovation was 3 σ_p .

Point 2: The RAS scheme performed without any problems for convective point 1, *now* the background state is almost saturated throughout all the column (see Fig. 2) and deserves a special attention.

In order to assess the behavior of the RAS scheme in presence of large innovations for such a convective regime, we look at the minimization results using a 100 % increase of precipitation for the observation as compared to the background. Figure 8 shows that the minimization still converges. The norm of the gradient has been reduced by 3 orders of magnitude. Note that now the amplitude of the analysis increments for T and q are more significant and compares with their respective standard-deviation errors specified for the background. The most significant aspect however is the appearence of a supersaturated layer with a definite vertical structure and might reflect a very specific process appearing within the RAS scheme.

We have not tried to isolate the source of this mechanism however. Our concern here is rather to point out that (in the same way as the "b" parameter for the Kuo scheme which was allowed to be negative) there appears to be *no mechanisms* within the RAS scheme (at least the version we are using here) to avoid consideration of vertical profiles that show significant supersaturation. It must be realized however that within a regular model time step, the RAS scheme may have to deal with supersaturated input profiles produced by the dynamics. This has clearly an implication in the present context (or more general 3D-Var or 4D-Var contexts). That is, for cases like the present one where the background state is (throughout the column) close to saturation and the ratio of the amplitude of the innovation over the standard-deviation error for the precipitation-rate is large, there is the possibility that the minimization produces significant supersaturation since; (1) the RAS scheme does not preclude it, and (2) the background term *can* allow it within the prescribed statistics. The conclusion here is that *we need to explicitly constrain supersaturation during the minimization with the RAS scheme in general to avoid large supersaturation in the resulting analysis fields.*

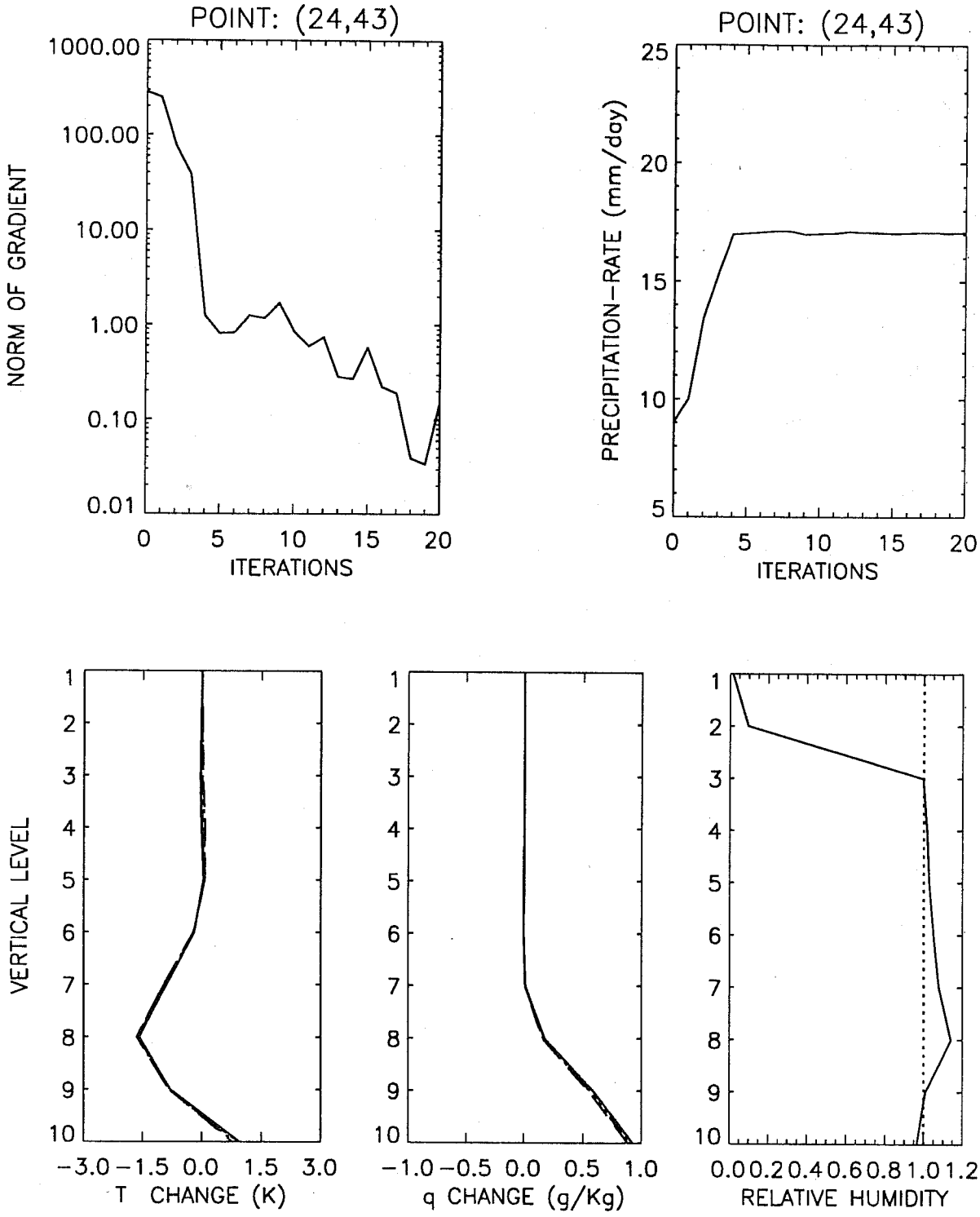

Fig. 8. 1D-Var minimization for point 2 located at I-J grid-coordinates (24, 43) for the RAS scheme.The precipitation-rate observation was 100 % larger than the background value.

Point 3: *Impact of the vertical correlation-scale L_T*:

We finally give a clear example showing the impact of the vertical correlation-scale of the background-error for the temperature field using the RAS scheme at the convective point 3. This is another typical convective regime close to the cold front but where both schemes agree more or less on the vertical distribution of heating (ref. Fig.3, point (19, 41)). Note from Fig. 2 that this time, the vertical profile is not close to saturation except in the upper part of the column. Figure 9a shows the diagnostics of the adjustment. The norm of the gradient is also significantly reduced by 4 to 5 orders of magnitude. These results were obtained using a correlation-scale $L_T = 0.1$.

We can physically expect a significant impact of increasing the correlation-scale for T since the 1D-Var results obtained so far with the RAS scheme typically produce analysis increments which are *positive* at the lowest level and *negative* for levels just above. This vertical decrease of the T change with height has the effect of *increasing* the convective instability. Increasing L_T to a critical value has the effect of forcing analysis increments of T with a smaller vertical slope and thus *reducing* the convective instability. Increasing the correlation-scale tends to counteract the destabilizing effect that the RAS scheme is typically using for increasing the precipitation-rate (i.e. convection). Increasing L_T to 0.2 produces analogous results as with $L_T = 0.1$. Increasing L_T to 0.3 *now* produces a significant transition in the vertical structure of the analysis increments; i.e., the T structure is very different. The results of the minimization are presented in Fig. 9b. The norm of the gradient has been well reduced by three orders of magnitude. Also, (as in the previous figures) the long-dashed curve indicates the analysis increment at iteration 7 and we can see that the convergence is to a *very* different vertical temperature distribution as compared to the $L_T = 0.1$ or 0.2 cases. The present structure appears more *barotropic* and looks more like the structure usually obtained with the Kuo scheme (which is not as sensitive to L_T). Also we observe that the final precipitation-rate is almost identical to that obtained in the previous experiment with $L_T = 0.1$ at the same point.

The same conclusions as those obtained for point 1 apply for point 4.

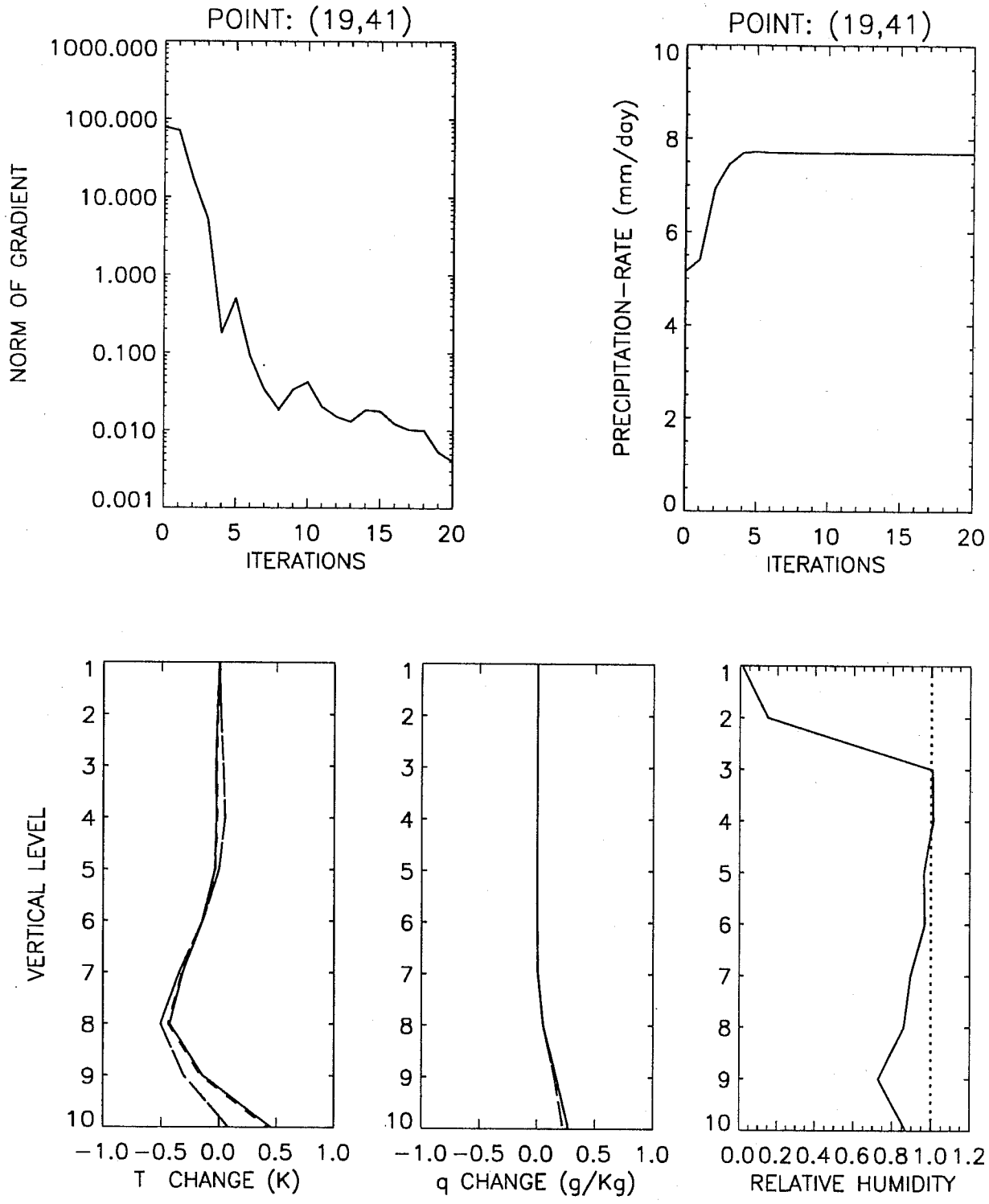

Fig. 9a. 1D-Var minimization for point 3 located at I-J grid-coordinates (19, 41) for the RAS scheme using a vertical correlation-scale L_T of 0.1.

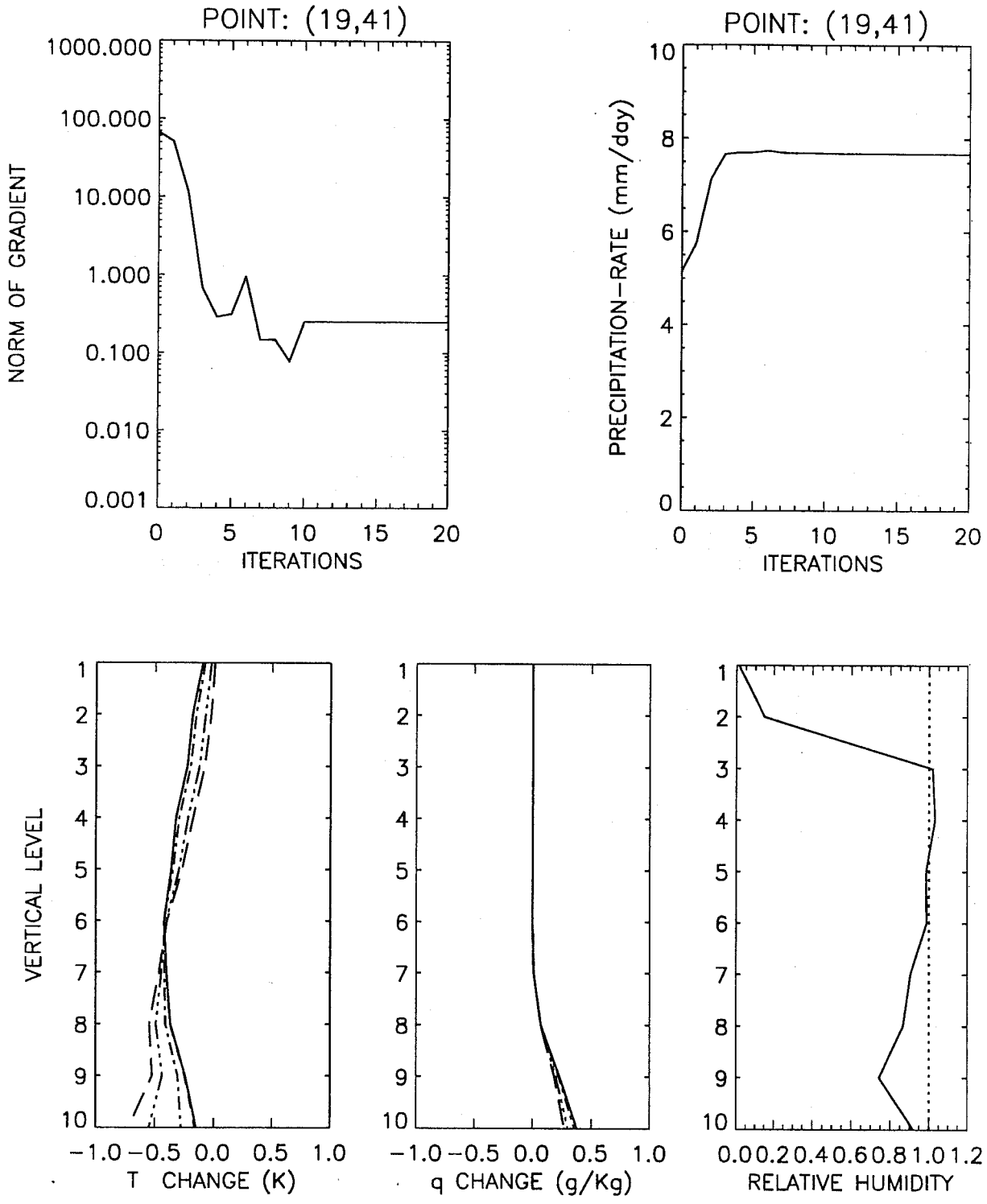

Fig. 9b. As in Fig. 9a but using a larger vertical correlation-scale L_T of 0.3 instead of 0.1 for the temperature field.

6. Summary and discussion

In this paper we have considered some basic aspects of the problem of variational assimilation of instantaneous precipitation-rate data using moist-convective parameterization schemes in a one-dimensional context. Two convective schemes were examined: a Kuo-Anthes scheme used at the National Center for Atmospheric Research (NCAR) and the Relaxed Arakawa-Schubert (RAS) scheme from the Data Assimilation Office (DAO/NASA). In view of wider applications to 3D-Var or 4D-Var, a 1D-Var scheme was formulated that contains the essential aspects of the vertical adjustment of temperature and specific-humidity fields at a given observation location in space. Realistic background fields and error statistics were specified. A systematic exploration of the nature of the adjustment was done at *non-pathological* convective points (i.e., points where the minimization remains in a convective regime throughout the minimization) for four typical convective regimes. The main conclusions are:

Sensitivity: The sensitivity of heating-rates due to perturbations of the temperature field and moisture field respectively (i.e., T-T and T-q Jacobian blocks matrices) appeared mostly *diagonal* at the upper analysis levels with the RAS scheme but also very sensitive at all vertical levels to perturbations at the lowest levels. Significant off-diagonal (low-level) sensitivity for the T-T sensitivity and moistening-rate due to specific-humidity perturbations appeared with the RAS scheme and is consistent with convective stability arguments. A significant off-diagonal structure of the T-T and T-q sensitivities was observed with the Kuo-Anthes scheme and simply reflects Anthes's assumption of parabolic distribution of the heating-rate in the vertical.

Nonlinearity: A Monte Carlo approach was used where thousands of different perturbation structure on temperature and specific-humidity based on the eigenvectors and eigenvalues of the background-error covariance matrix were generated. This method allowed an examination of nonlinearities in a realistic region of phase-space. For perturbation amplitudes of the order of the background-error standard deviations (i.e., typically those statistics used operationally for 6 h

forecast errors), the relative-error in the tangent-linear approximation for both schemes was found to be of the order of 100 % ; i.e., as large as the signal itself. A one-order reduction of the amplitude of these Monte Carlo perturbations (still with the same structure) reduces the error by one order of magnitude for the RAS scheme (a little more at high vertical levels) and by two orders of magnitude for the Kuo scheme. Judging from the amplitude of the changes done by the minimization at each iterations, this shows that the estimation of the gradient of the functional is typically 10 % in error during most of the minimization process.

Diagnostics of 1D-Var adjustments: 1- For background states close to saturation at the lowest vertical levels or even worse throughout the column, the minimization with the Kuo scheme requires a regularization (smoothing) for the specification of the partition parameter "b" as defined in Anthes et al. (1987). *2-* The RAS scheme was shown to allow a significant increase of precipitation-rate without signs of minimization problems. In a 3D-Var or 4D-Var context using the Kuo scheme, it is possible to consider the adjustment of the divergence field also in the minimization in order to increase the moisture accession locally. The conclusions obtained here on the vertical structure of the 1D-Var analysis increments would still apply since the moisture accession only affect the amplitude but not the vertical structure of the convective response. This would also be the case without "Anthes's approximation" on the shape of the vertical heating-rate. *3-* For the majority of cases examined, 5 iterations were sufficient to achieve convergence of 1D-Var for both schemes (most of the time 3 is enough).

4- When the background state is already close to saturation throughout most of the lowest part of the column, it is not recommended to use the RAS scheme (at least the version we're using) *without* constraining supersaturation in the analysis fields since there appears to be no mechanisms to avoid consideration of unrealistically large supersaturated states. This is similar to allowing the "b" parameter of the Kuo scheme to become negative without control on supersaturation. This aspect could be clearly isolated within the 1D-Var context but would presumably be difficult in more complex variational schemes where moist-convection is followed by large-scale precipitation processes which precipitates all moisture in excess of saturation and normally applied at the end of

a model timestep. An explicit control on supersaturation appears necessary. 5- For the RAS scheme, at a critical value of the background-error correlation-scale for temperature, more precisely 0.3 in σ-coordinates, under the same conditions for the other parameters of the problem, a transition occured where a different vertical structure of the analysis increment for the temperature field was obtained; i.e., a more *barotropic* structure was forced. This has implications for dynamical balance since the shallower specification of the correlation-scale means that with the RAS scheme, the analysis increments would apparently excite more internal gravity-modes in a more general context such as in 3D-Var or 4D-Var. The appropriate specification of background-error correlation scales needs to be explored using real forecast-error samples. Little is know on this aspect presently.

Acknowledgements. Thanks are due to Dr. Xiaolei Zou from the Mesoscale and Microscale Meteorology Division at NCAR for useful discussions and for kindly providing us with the computer code for the Kuo-Anthes scheme together with a version of the associated tangent-linear and adjoint schemes. Dr. Max Suarez from the Data Assimilation Office (DAO)/NASA kindly made available to us a version of the RAS scheme. Kevin Raeder from the Climate and Global Dynamics Division at NCAR provided the background fields from MAMS1 forecasts used in this study.

REFERENCES

Anthes, R. A., E.-Y. Hsie, and Y.H. Kuo, 1987: Description of the Penn State/NCAR Mesoscale Model Version 4 (MM4). NCAR/TN-282+STR, 66p. [Available from the National Center for Atmospheric Research, P.O. Box 3000, Boulder, Co, 80307, U.S.A.]

Daley, R., 1991: *Atmospheric data analysis.* Cambridge University Press. 457 pp.

Davidson and K. Puri, 1992: Tropical prediction using dynamical nudging, satellite-defined convective heat sources, and a cyclone bogus. *Mon. Wea. Rev.*, **120**, 2501-2522.

Deblonde, G., L. Garand, P. Gauthier, and C. Grassoti, 1995: Assimilation of SSM/I and GOES Humidity Retrievals with a One-dimensional Variational Analysis Scheme. *J. Appl. Meteor.*, **34**,1536-1550.

Donner, L. J., 1988: An initialization for cumulus convection in numerical weather prediction models. *Mon. Wea. Rev.*, **116**, 377-385.

Ehrendorfer, M., and R. Errico, 1995: Mesoscale predictibility and the spectrum of optimal perturbations. *J. Atmos. Sci.*, **52**, 3575-3500.

Errico, R., K. Raeder, and T. Vukicevic, 1994: Mesoscale Adjoint Modelling System, Version 1. NCAR Technical Note, NCAR/TN-410+IA. Climate and Global Dynamics Division, 214 pp. [Available from the National Center for Atmospheric Research, P.O. Box 3000, Boulder, Co, 80307, U.S.A.]

Garand, L. and C. Grassoti, 1995: Toward an objective analysis of rainfall rate combining observations and short-term forecast model estimates. *J. Appl. Meteor.*, **34**, 1962-1977.

Geleyn, J.F., 1985: On a simple, parameter-free partition between moistening and precipitation in the Kuo scheme. *Mon. Wea. Rev.*, **113**, 405-407.

Gilbert, J. C. and Lemaréchal 1989: Some numerical experiments with variable-storage quasi-Newton algorithms. *Mathematical Programming*, **45**, 407-435.

Gill, P.E., W. Murray, and M.H. Wright, 1981: *Practical Optimization*, Academic Press, 401 p.

Grassoti, C. and Garand, L., 1994: Classification-based rainfall estimation using satellite data and numerical forecast model fields. *J. Appl. Meteor.*, **33**, 159-178.

Heckley, W. A., G. Kelly, M. Tiedtke, 1990: On the use of Satellite-Derived Heating Rates for Data Assimilation within the Tropics. *Mon. Wea. Rev.*, **118**, 1743-1757.

Kasahara, A. and A. Mizzi, 1994: Diabatic initialization for improvement in the tropical analysis of divergence and moisture using satellite radiometric imagery data. *Tellus*, **46A**, 242-264.

_____, J.I. Tsutsui and H. Hirakuchi, 1996: Inversion Methods of Three Cumulus Parameterizations for Diabatic Initialization of a Tropical Cyclone Model. *Mon. Wea. Rev.*, **124**, 2304-2321.

Krishnamurti, T.N., K. Ingles, S. Cocke, T. Kitade, and R. Pasch, 1984: Details of low latitude medium range numerical weather prediction using a global spectral model. *J. Meteor. Soc. Japan*, **26**, 613-649.

_____, H.S., Bedi, and K. Ingles, 1993: Physical initialization using SSM/I rain-rates. *Tellus*, **45A**, 247-269.

Kuo, H.L., 1974: Further studies of the parameterization of the influence of cumulus convection on large-scale flow. *J. Atmos. Sci.*, **31**, 1232-1240.

Manobianco, J., S.E. Koch, V.M. Karyampudi, and A. J. Negri, 1994: The impact of assimilating satellite-derived precipitation rates on numerical simulations of the ERICA IOP 4 Cyclone. *Mon. Wea. Rev.*, **122**, 341-365.

Moorthi, S., and M.J. Suarez, 1992: Relaxed Arakawa-Schubert: A Parameterization of Moist Convection for General Circulation Models. *Mon. Wea. Rev.*, **120**, 978-1002.

Norquist, D.C., and S.S. Chang, 1994: Diagnosis and Correction of Systematic Humidity Error in a Global Numerical Weather Prediction Model. *Mon. Wea. Rev.*, **122**, 2442-2459.

Parrish, D.F., and J.C. Derber, 1992: The National Meteorological Center's spectral statistical interpolation analysis system. *Mon. Wea. Rev.*, **120**, 1747-1763.

Phalippou, L., 1996: Variational retrieval of humidity profile, wind speed and cloud liquid-water path with the SSM/I: Potential for numerical weather prediction. *Q. J. R. Meteorol. Soc.*, **122**, 327-355.

Raymond, W.H., W. S. Olson, and G. Callan, 1995: Diabatic Forcing and Initialization with Assimilation of Cloud Water and Rainwater in a Forecast Model. *Mon. Wea. Rev.*, **123**, 366-382.

Ritchie, H., 1991: Application of the semi-Lagrangian method to a multilevel spectral primitive-equations model. *Q. J. R. Meteorol. Soc.*, **117**, 91-106.

Tarantola, A. 1987: *Inverse Problem Theory*. Amsterdam, Elsevier. 613 p.

Tsuyuki, T., 1996a: Variational Data Assimilation in the Tropics Using Precipitation Data, Part I: Column model. *Meteor. Atmos. Phys.*, Vol **60**, 87-104.

_____, 1996b: Variational Data Assimilation in the Tropics Using Precipitation Data, Part II: 3-D model. *Mon. Wea. Rev.*, **124**, 2545-2561.

Turpeinen, O. M., L. Garand, R. Benoit, and M. Roch, 1990: Diabatic initialization of the Canadian regional finite-element (RFE) model using satellite data. Part I: Methodology and application to a winter storm. *Mon. Wea. Rev* , **118**, 1381-1395.

Vukicevic, T., and R. M. Errico, 1993: Linearization and adjoint of parameterized moist diabatic processes. *Tellus*, **45A**, 493-510.

Xu, Q., 1996a: Generalized Adjoint for Physical Processes with Parameterized Discontinuities. Part I: Basic Issues and Heuristic Examples. *J. Atmos. Sci.*, **53**, 1123-1142.

_____, 1996b: Generalized Adjoint for Physical Processes with Parameterized Discontinuities. Part II: Formulations and matching Conditions. *J. Atmos. Sci.*, **53**, 1143-1155.

Zou, X., I. M. Navon, and J. Sela, 1993: Variational data assimilation with moist threshold processes using the NMC spectral model. *Tellus*, **45A**, 370-387.

Zupanski, D., 1993: The effects of discontinuities in the Betts-Miller cumulus convection scheme on four-dimensional variational data assimilation. *Tellus*, **45A**, 511-524.

_____, and F. Mesinger, 1995: Four-Dimensional Variational Assimilation of Precipitation Data. *Mon. Wea. Rev.*, **123**, 1112-1127.